

1 Supporting information for: Wilson *et al.* 2022. The role of spatial
2 structure in at-risk metapopulation recoveries. In: *Ecological*
3 *Applications*.

4 **Appendix S1:** Overview of metapopulation model description & detailed results

5 Kyle L. Wilson^{1,2*}, Alexandra C. Sawyer¹, Anna Potapova¹, Colin J. Bailey¹, Daniella LoScerbo^{3,4},
Elissa K. Sweeney-Bergen^{1,5}, Emma E. Hodgson^{1,4}, Kara J. Pitman¹, Karl M. Seitz¹,
Lauren Law^{1,6}, Luke Warkentin^{1,7}, Samantha M. Wilson¹, William I. Atlas^{1,8},
Douglas C. Braun^{3,5}, Matthew R. Sloat⁸, M. Tim Tinker⁹,
and Jonathan W. Moore^{1,3}

¹Earth to Ocean Research Group, Simon Fraser University

²Central Coast Indigenous Resource Alliance, Campbell River, BC

³Resource and Environmental Management, Simon Fraser University

⁴Fisheries & Oceans Canada, Cultus Lake Laboratory, Cultus Lake, BC

5Ministry of Forests, Lands, Natural Resource Operations, and Rural Development, Smithers, BC

⁶Fisheries & Oceans Canada, Salmonid Enhancement Program, Nanaimo, BC

⁷Fisheries & Oceans Canada, North Coast Stock Assessment, Smithers, BC

⁸Wild Salmon Center, Portland, OR

⁹Ecology and Evolutionary Biology, University of California Santa Cruz

6 16 December 2022

7 **Contents**

S1.1 Metapopulation model	3
S1.1.1 Local & metapopulation dynamics	3
S1.1.2 Creating the spatial networks	4
S1.1.3 Dispersal	5
S1.1.4 Disturbance regimes	6
S1.1.5 Recruitment stochasticity	7
S1.2 Post-disturbance outcomes	8
S1.2.1 Monitoring & management at aggregate-scale	8
S1.2.2 Recovery metrics	9
S1.3 Scenarios	9
S1.3.1 Walkthrough of example results	11
S1.4 Sensitivity test of mean recovery metrics	17
S1.5 General patterns	18
S1.5.1 Effects of disturbance regime	18
S1.5.2 Role of interplay in ecological and disturbance conditions on recovery patterns	19
S1.6 Clustering analyses	24
S1.6.1 Emergent recovery outcomes	25

*Corresponding author - email: klwilson.ccira@gmail.com

²⁵	S1.6.2 Role of ecological and disturbance conditions on recovery outcomes	27
²⁶	S1.7 References	29

²⁷ **S1.1 Metapopulation model**

²⁸ **S1.1.1 Local & metapopulation dynamics**

²⁹ Our metapopulation was defined by a set of P local populations for a species with a one year generation time with
³⁰ time-dynamics that follows birth (i.e., recruitment R), immigration, death, and emigration processes typical to
³¹ metapopulation theory and tested the role of multiple local and regional processes (Anderson *et al.* 2015; Fullerton
³² et al. 2016; Zelnik *et al.* 2019; Bowlby & Gibson 2020; Okamoto *et al.* 2020):

$$N_{i,t} = (1 - d_{i,t})(R_{i,t} + \sum_{\substack{j=1 \\ j \neq i}}^P \omega p_{i,j} R_{j,t} - \omega R_{i,t}) \quad (\text{S.1})$$

³³ where $N_{i,t}$ was the number of adults in patch i at time t , $R_{i,t}$ was the number of recruits at time t , $\sum_{\substack{j=1 \\ j \neq i}}^P \omega p_{i,j} R_{j,t}$ was
³⁴ the number of recruits immigrating into patch i from any other patch, ω was the proportion of local recruits to
³⁵ disperse, $p_{i,j}$ was a distance-dependent dispersal function, and $d_{i,t}$ was the proportion of post-dispersal recruits lost
³⁶ from the disturbance regime.

³⁷ Figure S1 shows how local patch recruitment at time t depended on adult densities at $t-1$ and followed a
³⁸ reparameterized Beverton-Holt function based on compensation ratio (see Box 3.1 in Walters & Martell 2004) and
³⁹ ignoring age-structure to model adult-to-adult dynamics, i.e., setting $\phi_{E_0} = 1$, $\phi_{B_0} = 1$ and $R_0 = N_0$ (see Table 3 in
⁴⁰ Forrest *et al.* 2010):

$$R_{i,t} = \frac{\alpha_i N_{i,t-1}}{1 + \frac{\alpha_i - 1}{\beta_i} N_{i,t-1}} \epsilon_{i,t} \quad (\text{S.2})$$

⁴¹ where α_i was the recruitment compensation ratio, β_i was local patch carrying capacity, and $\epsilon_{i,t}$ was lognormally
⁴² distributed deviates to introduce stochastic recruitment dynamics.

⁴³ Resource monitoring often occurs at the scale of the whole metapopulation by sampling aggregate abundances from
⁴⁴ multiple local populations to (Anderson *et al.* 2015; Moore *et al.* 2021), hence we define metapopulation adults as:

$$A_t = \sum_{i=1}^P N_{i,t} \quad (\text{S.3})$$

⁴⁵ with metapopulation recruits:

$$K_t = \sum_{i=1}^P R_{i,t} \quad (\text{S.4})$$

⁴⁶ Monitoring at the scale of the whole metapopulation can produce productivity relationships that aggregates the
⁴⁷ population dynamics and productivity among all local populations. For example, take a two patch metapopulation
⁴⁸ model (Figure S1) that each vary in demographic shape parameters $\alpha_1 = 2$; $\alpha_2 = 4$ and $\beta_1 = 100$; $\beta_2 = 200$. Here,
⁴⁹ recruitment compensation from local patches α_i gets averaged across the metapopulation leading to an average
⁵⁰ compensation ratio $\bar{\alpha}$ of 3. Likewise, the total carrying capacity of the metapopulation $\bar{\beta}$ becomes the summation
⁵¹ of local patch carrying capacities $\sum \beta_i$, which was 300. This scale of monitoring generates the following local patch
⁵² and metapopulation dynamics:

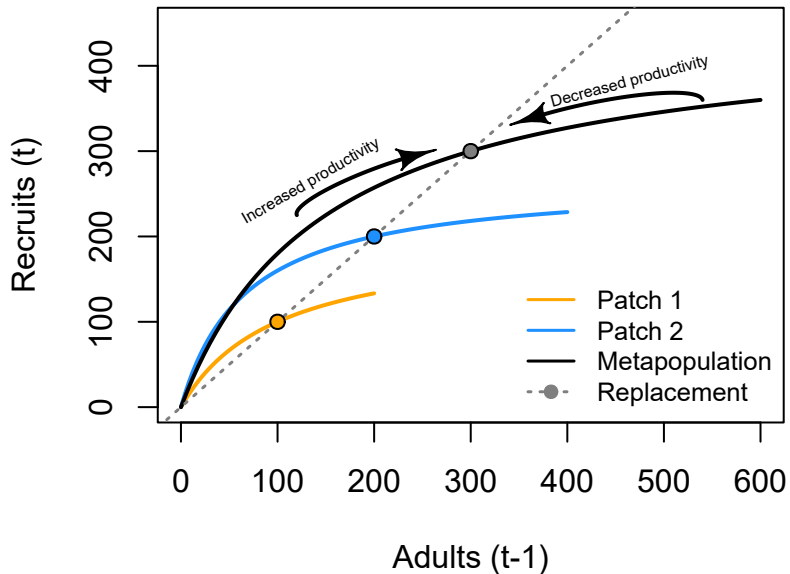


Figure S1: Density dependence in metapopulation and local patch recruitment dynamics. Dashed line indicates the line of replacement, with equilibrium indicated by points. When populations fall below equilibrium points, per-capita productivity improves driving populations back towards equilibrium. When populations exceed their capacity, per-capita productivity decreases driving populations back towards equilibrium. At each point of the x-axis, the distance between the solid and dashed lines indicates the amount of recruitment above replacement, i.e., the surplus recruitment produced via compensatory density dependence.

53 S1.1.2 Creating the spatial networks

54 The next aspect to developing our metapopulation model was connecting the set of patches to one another (Yeakel
 55 et al. 2014). We needed to specify the number of patches, their arrangements (i.e., connections), and how far apart
 56 they are from one another. We followed some classic metapopulation and source-sink arrangements to create four
 57 networks that generalize across a few real-world topologies: a linear habitat network (e.g., coastline), a dendritic or
 58 branching network (e.g., coastal rivers), a star network (e.g., mountain & valley, or lake with inlet tributaries), and
 59 a grid network (e.g., grasslands).

60 To make networks comparable, each spatial network type needs the same leading parameters (e.g., number of
 61 patches P and mean distance between neighboring patches \bar{d}). In this case, we set P to 16 and \bar{d} to 1 unit
 62 (distance units are arbitrary). We used the `igraph` package (Csardi & Nepusz 2006) to arrange our spatial
 63 networks as the following:

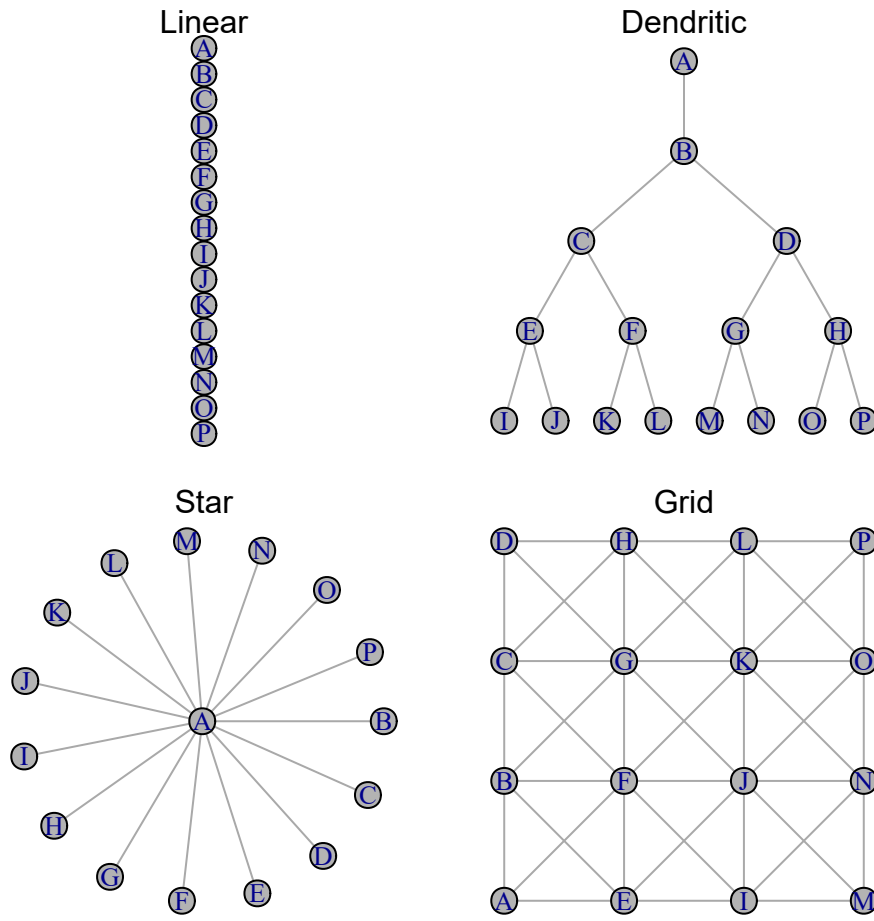


Figure S2: Four spatial network topologies.

64 Note that distances between neighbor patches in the above networks are equal. Table S1 shows an example
 65 dispersal matrix for a grid network.

66 S1.1.3 Dispersal

67 Dispersal from patch i into patch j depends on constant dispersal rate ω (defined as the proportion of total local
 68 recruits that will disperse) and an exponential distance-decay function between i and j with distance cost to
 69 dispersal m (Anderson et al. 2015; Fullerton et al. 2016):

$$E_{i,j,t} = \omega R_{i,t} p_{i,j} \quad (\text{S.5})$$

70 where $E_{i,j}$ was the total dispersing animals from patch i into patch j resulting from dispersal rate ω , total number
 71 of local recruits $R_{i,t}$, and probability of dispersal between patches $p_{i,j}$:

$$p_{i,j} = \frac{e^{-md_{i,j}}}{\sum_{\substack{j=1 \\ j \neq i}}^P e^{-md_{i,j}}} \quad (\text{S.6})$$

72 where $d_{i,j}$ was the pairwise distance between patches, m was the distance cost to dispersal. The summation term in

Table S1: Example distance matrix between 16 patches within a grid network to affect distance-dependent dispersal rates.

	A	B	E	F	C	G	D	H	I	J	K	L	M	N	O	P
A	0	1	1	1	2	2	3	3	2	2	2	3	3	3	3	3
B	1	0	1	1	1	1	2	2	2	2	2	2	3	3	3	3
E	1	1	0	1	2	2	3	3	1	1	2	3	2	2	2	3
F	1	1	1	0	1	1	2	2	1	1	1	2	2	2	2	2
C	2	1	2	1	0	1	1	1	2	2	2	2	3	3	3	3
G	2	1	2	1	1	0	1	1	2	1	1	1	2	2	2	2
D	3	2	3	2	1	1	0	1	3	2	2	2	3	3	3	3
H	3	2	3	2	1	1	1	0	3	2	1	1	3	2	2	2
I	2	2	1	1	2	2	3	3	0	1	2	3	1	1	2	3
J	2	2	1	1	2	1	2	2	1	0	1	2	1	1	1	2
K	2	2	2	1	2	1	2	1	2	1	0	1	2	1	1	1
L	3	2	3	2	2	1	2	1	3	2	1	0	3	2	1	1
M	3	3	2	2	3	2	3	3	1	1	2	3	0	1	2	3
N	3	3	2	2	3	2	3	2	1	1	1	2	1	0	1	2
O	3	3	2	2	3	2	3	2	2	1	1	1	2	1	0	1
P	3	3	3	2	3	2	3	2	3	2	1	1	3	2	1	0

73 the denominator normalizes the probability of moving to any patch to between 0 and 1 with the constraint that
 74 dispersers cannot move back into their home patch (i.e., $j \neq i$. With $\bar{d} = 1$, $m = 0.5$, $\omega = 0.1$, $R_{i,t} = 100$ in a linear
 75 network):

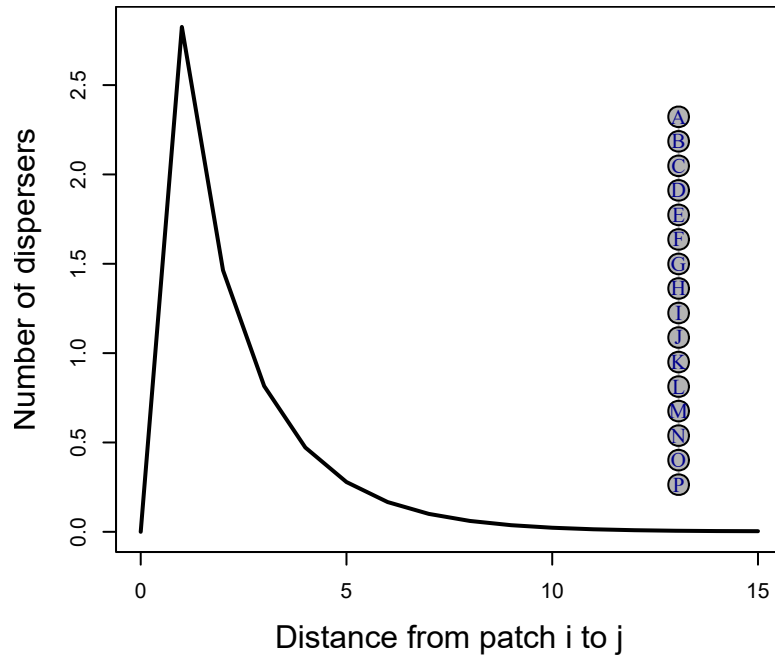


Figure S3: Example dispersal patterns across linear network.

76 S1.1.4 Disturbance regimes

77 In all scenarios, disturbance was applied after 50 years of equilibrating the metapopulation at pristine conditions.
 78 We then applied a pulsed disturbance regime at year 50 (the regime varied from *uniform*, *localized*, *even*, and

localized, uneven - see *Scenarios* below). Disturbance immediately removed a fixed proportion of the metapopulation adults at that time (i.e., 0.9 of $A_{t=50}$). Once applied, the metapopulation was no longer disturbed and spatio-temporal recovery dynamics emerged from these conditions given the ecological scenarios of network complexity, dispersal rate, spatio-temporal correlations, local patch demographies, and magnitude of stochastic variance.

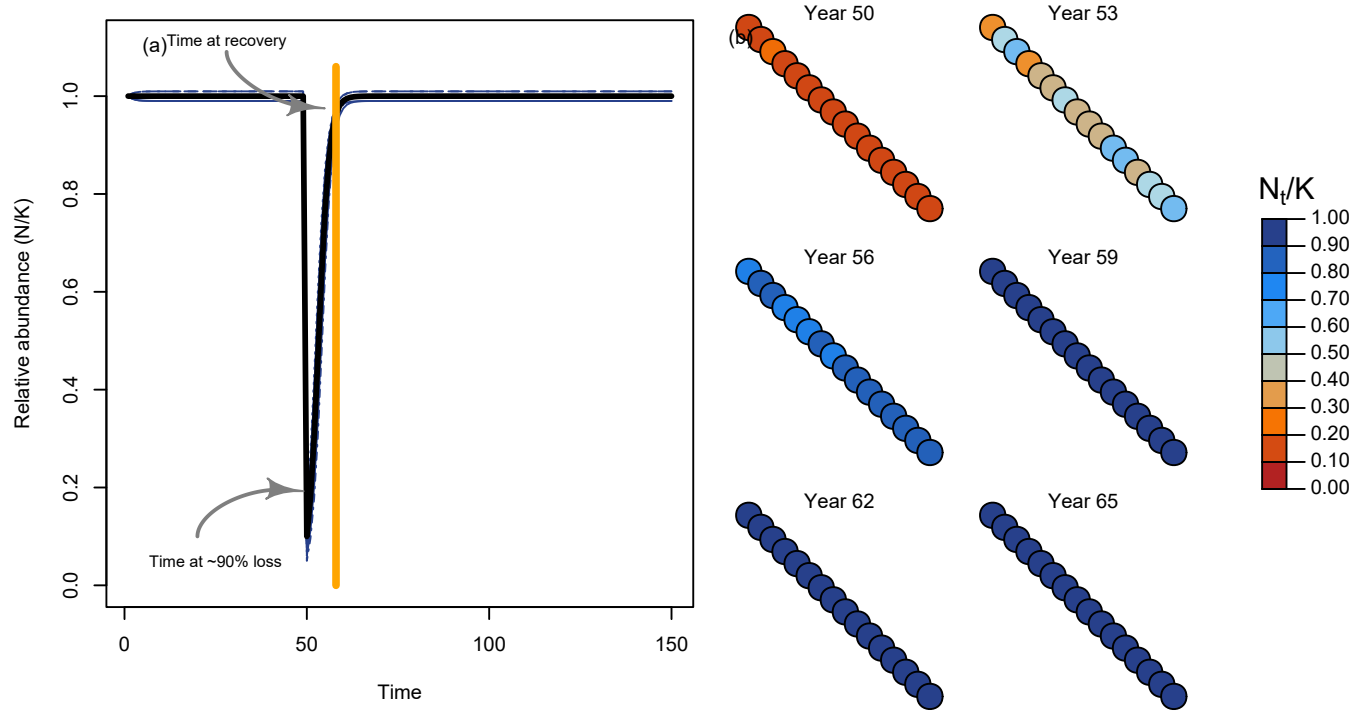


Figure S4: Recovery regime of metapopulation with linear topology through time (a) and space (b).

S1.1.5 Recruitment stochasticity

Our model allowed for stochastic recruitment that followed a lognormal distribution with average variation in recruitment of σ_R . In cases with stochastic recruitment, the deterministic recruitment in eq. S.4 becomes:

$$R_{i,t} = \frac{\alpha_i N_{i,t-1}}{1 + \frac{\alpha_i - 1}{\beta_i} N_{i,t-1}} e^{(\epsilon_{i,t} - \frac{\sigma_R^2}{2})} \quad (\text{S.7})$$

where lognormal deviates for each patch i at time t were drawn from a multivariate normal distribution (*MVN*) with bias correction $\frac{\sigma_R^2}{2}$. If σ_R was low, then metapopulation dynamics approach the deterministic case. In some scenarios, we evaluated the role of spatially and/or temporally correlated deviates among local patches to model potential common drivers affecting metapopulation dynamics (e.g., Moran effects). Expected recruitment deviates followed a first-order autoregression model such that:

$$\epsilon_{i,t} = \rho_T \epsilon_{i,t-1} + MVN(\mu = 0, \Sigma = \sigma_R^2 (1 - \rho_T^2) e^{-\rho_S D_{i,j}}) \quad (\text{S.8})$$

where ρ_T was temporal correlation (bounded 0 – 1) and ρ_S was rate of distance-decay in spatial correlation (bounded 0 – ∞ with higher values leading to independent patches). If ρ_T was 0 and ρ_S was high, then annual recruitment deviates were independent. We modelled the initial conditions for autoregressive recruitment deviates

⁹⁵ $\epsilon_{i,1}$ by drawing from a stationary normal distribution with mean $\mu = 0$ and variance σ_R^2 such that:

$$\epsilon_{i,1} \sim N(\mu = 0, \sigma = \sigma_R) \quad (\text{S.9})$$

⁹⁶ We illustrate the effects of four kinds of recruitment deviates below using the same random number generator seed:

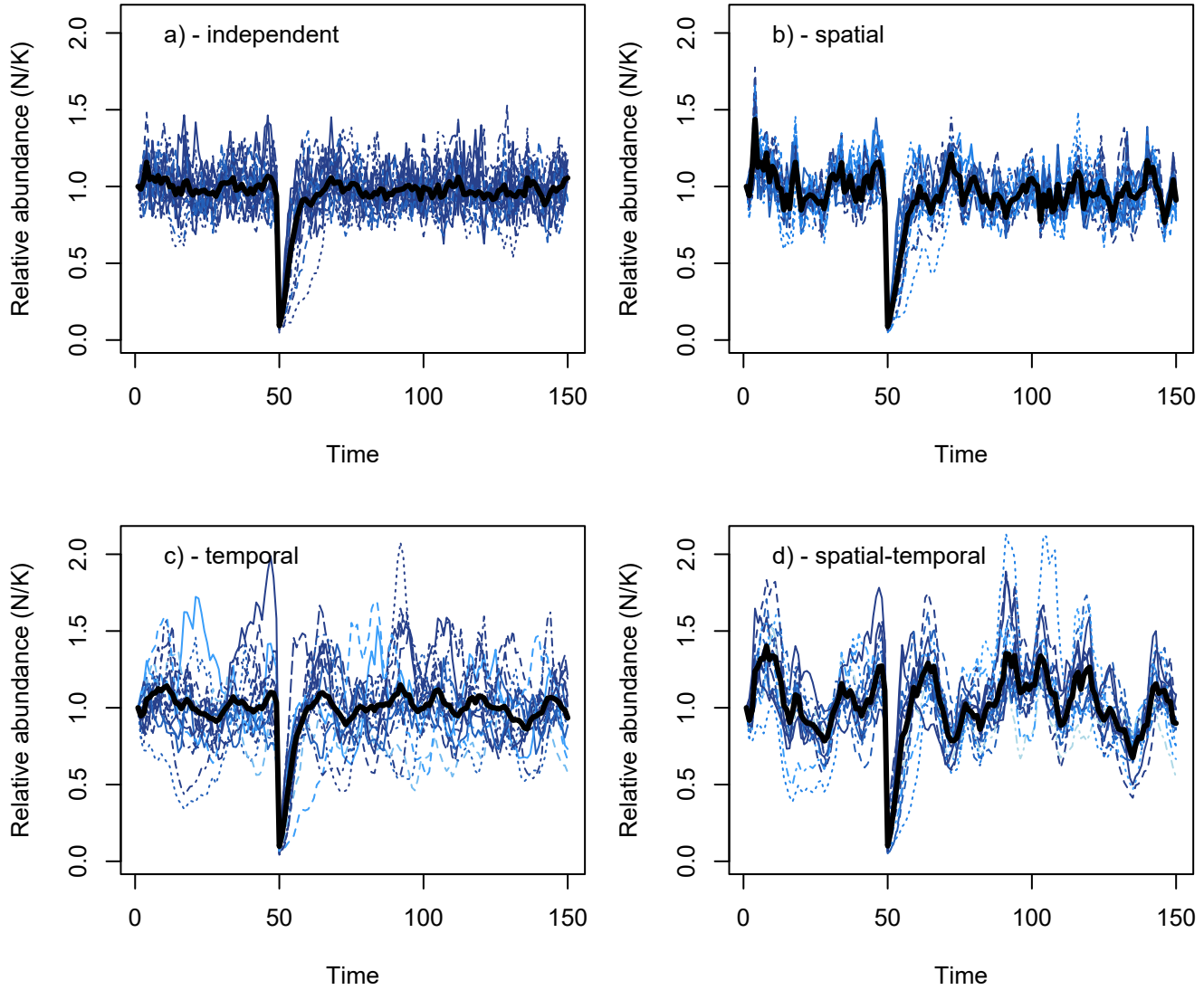


Figure S5: Metapopulation dynamics with independent (a), spatially correlated (b), temporally correlated (c), and spatio-temporally correlated (d) recruitment deviates. Black line indicates metapopulation, and dashed lines indicate local patches with red and blue relating to abundances after 100 years post-disturbance were less than or greater than 1.0 pre-disturbance, respectively.

⁹⁷ S1.2 Post-disturbance outcomes

⁹⁸ S1.2.1 Monitoring & management at aggregate-scale

⁹⁹ While true metapopulation dynamics emerge from local patch dynamics and dispersal in eq. S.1, natural resource
¹⁰⁰ managers often monitor and manage at the scale of the metapopulation. Hence, management at this scale
¹⁰¹ inherently defines the stock-recruitment dynamics of the aggregate complex of patches (i.e., metapopulation) as:

$$\mathbb{E}(N_t) = \frac{\bar{\alpha}A_{t-1}}{1 + \frac{\bar{\alpha}-1}{\bar{\beta}}A_{t-1}} \quad (\text{S.10})$$

where $\bar{\alpha}$ was the compensation ratio averaged across the metapopulation and $\bar{\beta}$ was the carrying capacity summed across the entire metapopulation.

104 S1.2.2 Recovery metrics

105 We measured the following post-disturbance outcomes to track the temporal and spatial recovery regime of the
106 metapopulation.

- 107 1. Recovery rate after disturbance: Recovery rate represents the inverse proportion of the post-disturbance
108 phase that the metapopulation took to recover. Recovery rate was calculated as $1 - T_{recovery}/T_{sim}$ where the
109 recovery time, $T_{recovery}$, was the number of years/generations (1 year = 1 generation in our models) it took
110 for the metapopulation to reach five consecutive years pre-disturbance abundance. Recovery rate captures
111 how quickly the aggregate metapopulation recovers from disturbance but doesn't take into account whether
112 any given local patches recover to their pre-disturbance capacity nor did it allow for any uncertainty around
113 recovery criteria.
- 114 2. Patch occupancy: The number of patches with >0.1 local carrying capacity after disturbance in the
115 short-term (5 years), medium-term (10 years), and long-term (25 years). This value characterizes the
116 expected risk of spatial contractions or local patch collapses, and reflects how interactions between spatial
117 structure, disturbance, and dispersal shape source-sink dynamics and the ability to provide (or not) rescue
118 effects and recover local patches.
- 119 3. Relative production: The ratio between the empirical metapopulation adult abundances to the expected
120 adult recruitment if the metapopulation were a single, contiguous population of equivalent size and
121 productivity (i.e., carrying capacities and productivity were equal to the sum β and mean α among patches,
122 respectively). We term Δ_N by calculating the stock-recruitment model to aggregate metapopulation adults
123 (eq. S.10) such that:

$$\Delta_{N_t} = \frac{A_t}{\mathbb{E}(N_t)} \quad (\text{S.11})$$

124 A value of 1.0 would indicate that the disturbed metapopulation production was equal to a single, contiguous
125 population such that source-sink dynamics were not consuming surplus recruits. In other words, this metric
126 can describe whether the metapopulation acts more than ($\Delta_{N_t} > 1.0$), less than ($\Delta_{N_t} < 1.0$), or equal to the
127 sum of its parts ($\Delta_{N_t} = 1.0$).

- 128 4. Risk of non-recovery after disturbance: Non-recovery rate was defined as the % of simulations where
129 metapopulation abundance failed to recover to 1.0 of the average pre-disturbance abundance for 5
130 consecutive years post-disturbance. This "non-recovery rate" reflects the risk of a long-term state shift in
131 metapopulation dynamics after disturbance in the face of stochasticity.

132 S1.3 Scenarios

133 We tested all combinations of the following eight processes (below) and ran 100 stochastic iterations per scenario
134 (see section on *Sensitivity test of mean recovery metrics* below) to estimate the mean outcome for each of the above
135 recovery metrics:

- 136 1. Homogenous and spatially variable recruitment compensation ratio across patches, i.e. intrinsic rate of
137 population growth (α_i).
 - 138 a. when **variable**, $\alpha_i \sim TN(\mu = \bar{\alpha}, \sigma_\alpha = 0.3\bar{\alpha})$ with a truncation applied such that $5 \leq \alpha_i \geq 1$ to ensure
139 that patches could, at minimum, replace themselves but with an upper limit of a 5-fold
140 improvement to per-capita productivity. By comparison, Myers *et al.* (1999) found that compensation

ratio (their $\hat{\alpha}$) ranged 1-7 for most species evaluated. Since our focus was on at-risk species, we opted to truncate α_i towards the lower end of this range, with a mean of 2.0.

2. Homogenous and spatially variable local carrying capacity across patches, i.e. asymptote of expected recruits at high adult densities (β_i)

- a. when **variable**, $\beta_i \sim \text{multinomial}(p_i, N)$ where $p_i = \frac{e^{\theta_i}}{\sum e^{\theta_i}}$, $\theta_i \sim \text{uniform}(0, 1)$, and $N = \bar{\beta}$, with the added constraint that $\beta_i < 0.1\bar{\beta}$ to ensure that no one patch exceed 10% of total metapopulation abundance (a necessary constraint when modelling *local, even* and *local, uneven* disturbances below). Note that, when local variation in demography rates occurred, the truncated normal in Appendix S1: Section S1.3.1.a and truncated multinomial in Appendix S1: Section S1.3.2.a above led compensation ratio and carrying capacity, respectively, to vary by the same magnitude ~28% coefficient of variation (Appendix S1: Figure S6).

3. Variation in the spatial distribution of disturbances where a proportion of individuals were removed from the metapopulation (e.g., 0.90) occurs.

- a. *uniform* - individuals randomly removed across all patches, with all individuals having equal vulnerability to being removed.
- b. *local, even* - randomly chosen individuals removed from random subset of patches (as long as the target individuals lost in the metapopulation can be achieved in that subset of patches)
- i. Specifically, a numerical algorithm was used to search and find a set of disturbance conditions whereby removing a random proportion of individuals from a random subset of local patches achieved both:
 - a total loss that summed to a ~90% loss in abundance to the whole metapopulation, and
 - left at least one local patch *undisturbed* to start metapopulation recoveries.
 - c. *local, uneven* - total extirpation of randomly selected subset of patches (as long as the target individuals lost in the metapopulation can be achieved in that subset of patches).
- i. Specifically, a numerical algorithm was used to search and find a set of disturbance conditions whereby extirpations to a random subset of local patches achieved both:
- a total loss that summed to a ~90% loss in abundance to the whole metapopulation, and
 - left at least one local patch *undisturbed* to start metapopulation recoveries.

4. Density-independent dispersal rates ω from 0 to 5% of individuals within a patch will disperse.
5. Topology of the spatial networks with linear, dendritic, star, and grid networks. Each network with $P = 16$ and distance between patches $\bar{d} = 1$.
6. Stochastic recruitment deviates with low, medium, and high standard deviation in lognormal error. Used to generate stochastic population dynamics via random deviates from the expected recruitment relationship in eq. S.2.
7. Temporal correlation in recruitment deviates from low, medium, and high correlation (i.e., good year at time t begets good year at time $t+1$).
8. Spatial correlation in recruitment deviates among patches from low, medium, to high correlation (i.e., neighboring patches go up or down together).

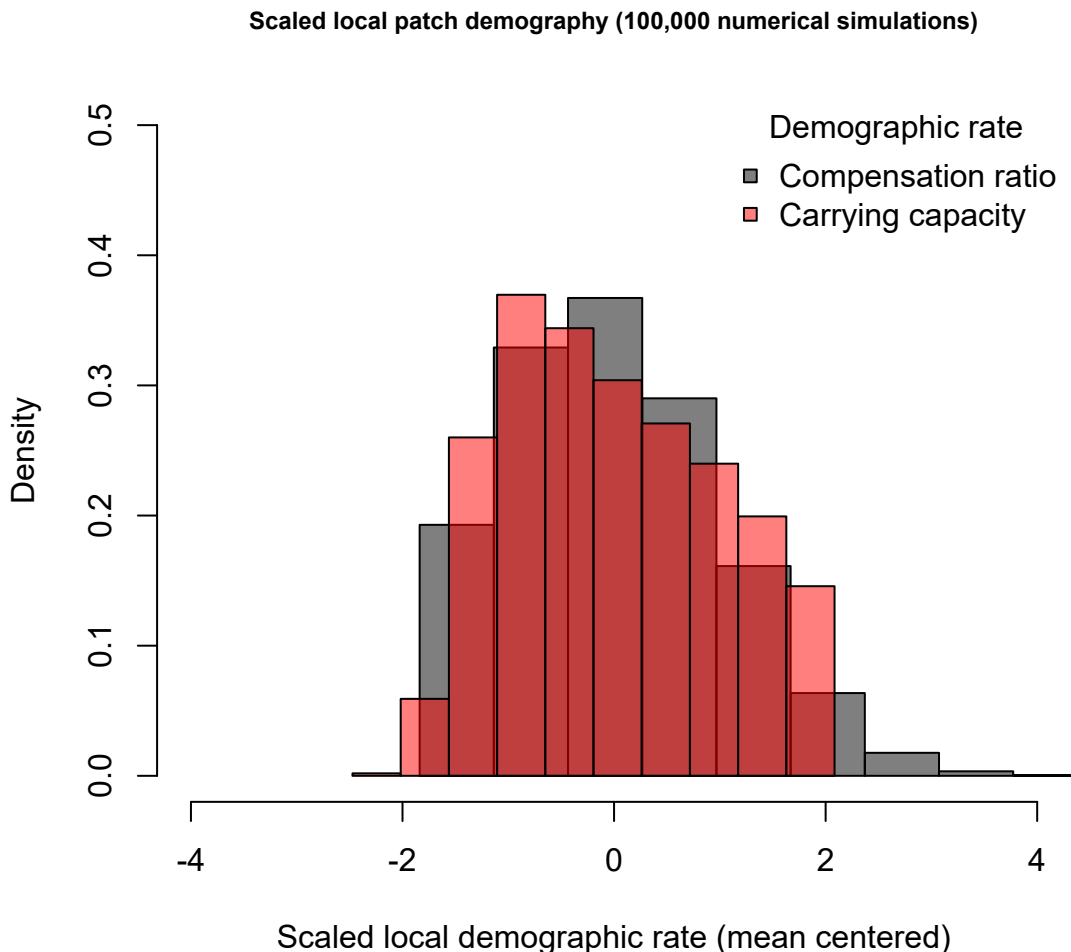


Figure S6: Histogram showing variation among demographic rates after simulating 100,000 local patches when using the truncated normal in Appendix S1: Section 1.3(1.a) and truncated multinomial in Appendix S1: Section 1.3(2.a) when modelling variation in local compensation ratio (grey) and carrying capacity (red).

¹⁷⁹ **S1.3.1 Walkthrough of example results**

¹⁸⁰ We demonstrate our metapopulation model with an example outcome for a linear network composed of 16 patches,
¹⁸¹ a dispersal rate of 0.01 and a high enough dispersal cost such that individuals are only willing to move to their
¹⁸² closest neighboring patches. This limits the strength of potential rescue effects. For this example, patches varied in
¹⁸³ their productivity and carrying capacity but will have deterministic population dynamics.

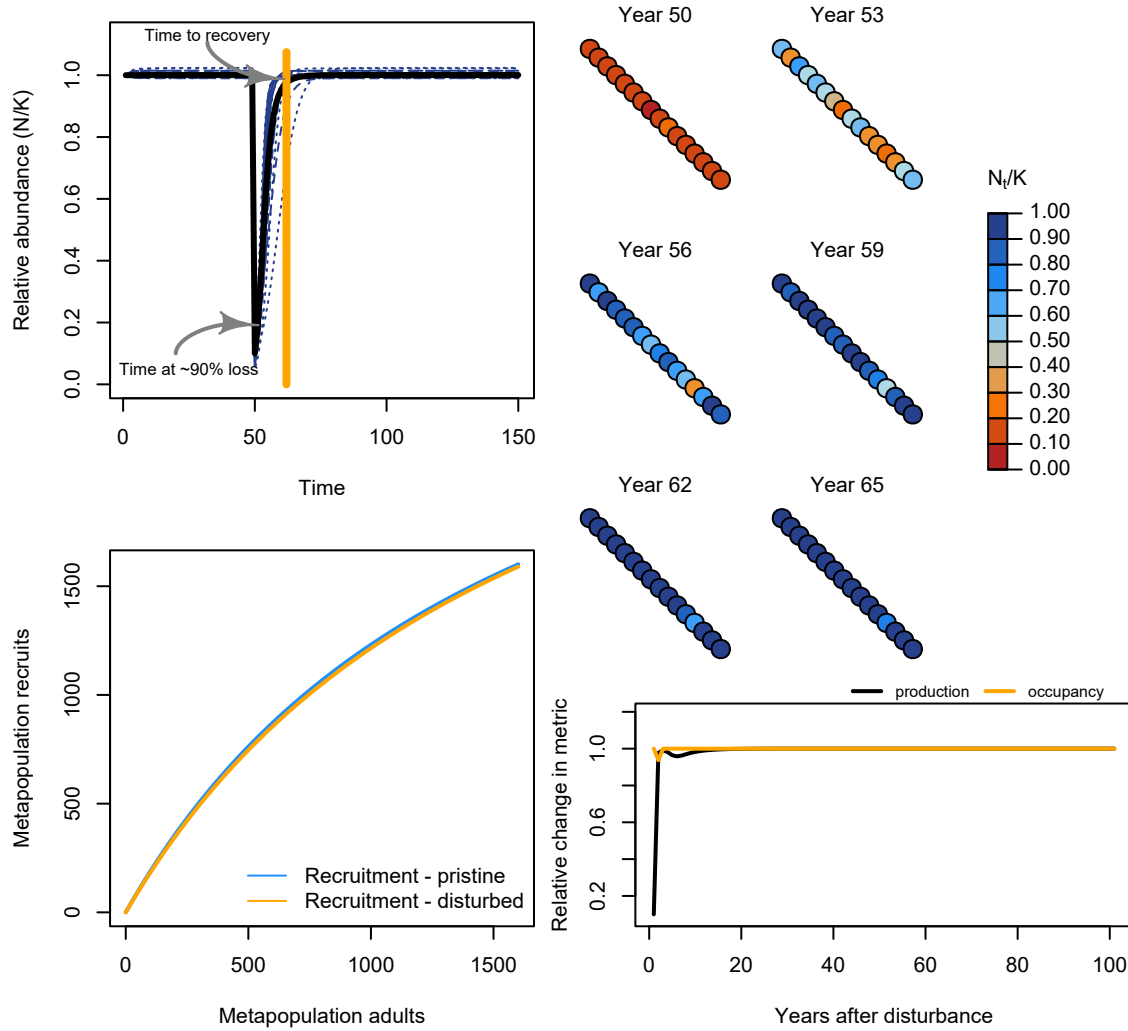


Figure S7: Example iteration of spatial recovery regime of metapopulation with linear topology through time (top left) and space (top right). Recruitment dynamics before and 10 years after disturbance (bottom left). Relative bias in aggregate-scale estimates of carrying capacity, compensation ratio, and recruitment production in recovery phase (bottom right).

¹⁸⁴ We can then contrast this with a different network shape, like a dendritic network.

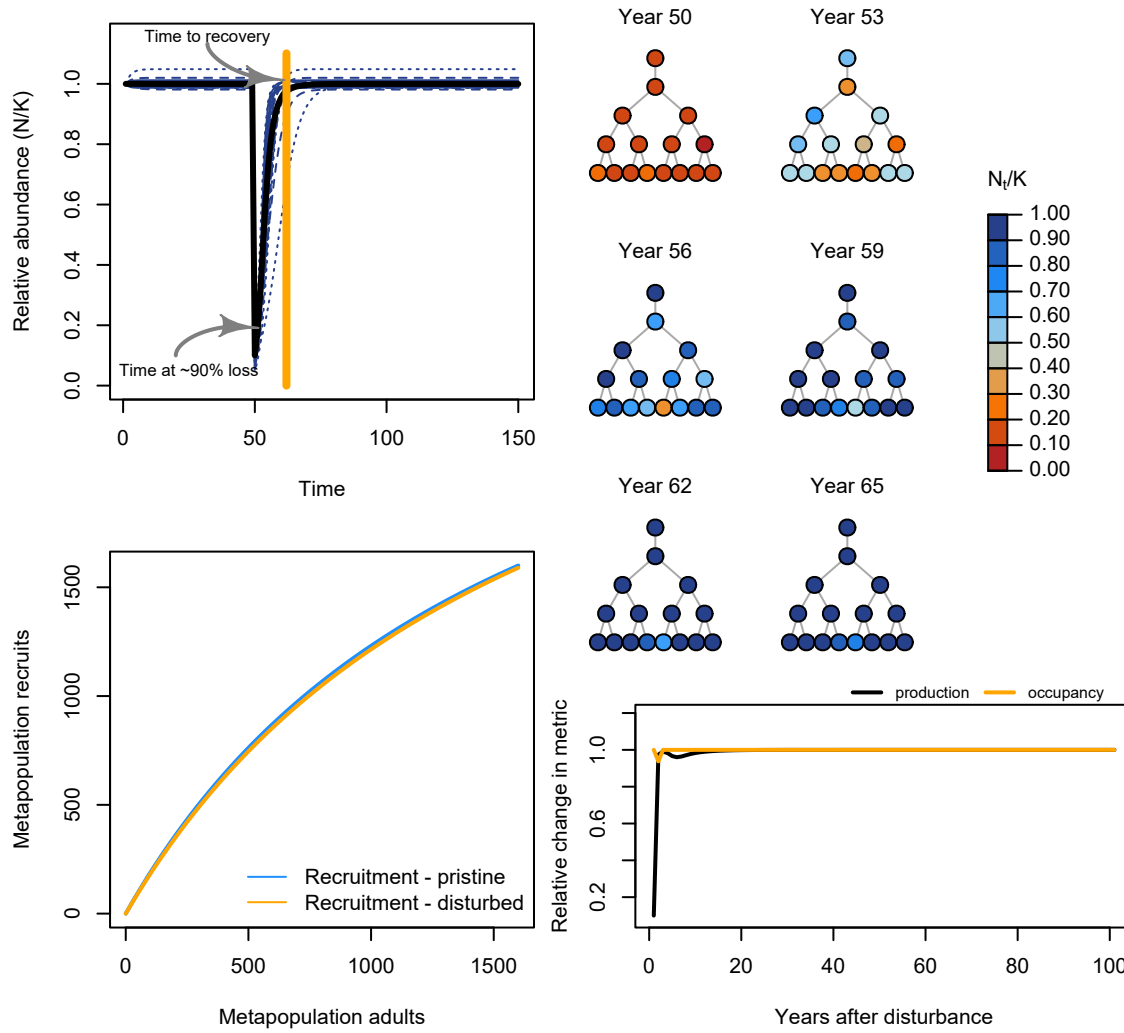


Figure S8: Example iteration of spatial recovery regime of metapopulation with dendritic topology.

¹⁸⁵ Now, let's add some stochasticity to recruitment and see how this affects the recovery regime.

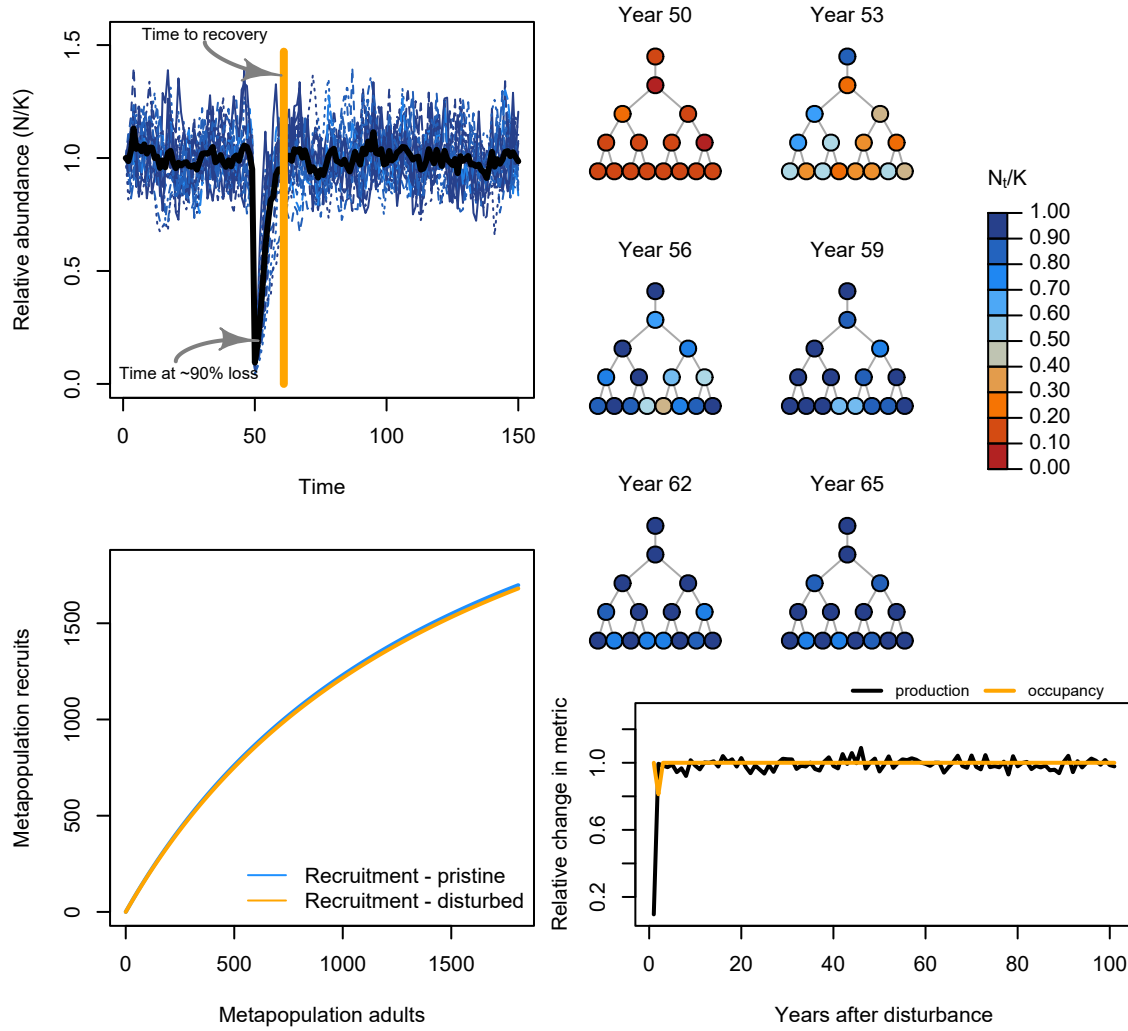


Figure S9: Example iteration of spatial recovery regime of stochastic metapopulation.

186 Next, we can contrast with a disturbance regime where the disturbance is locally even among a subset of local
 187 patches (rather than uniform across all patches or local extirpations).

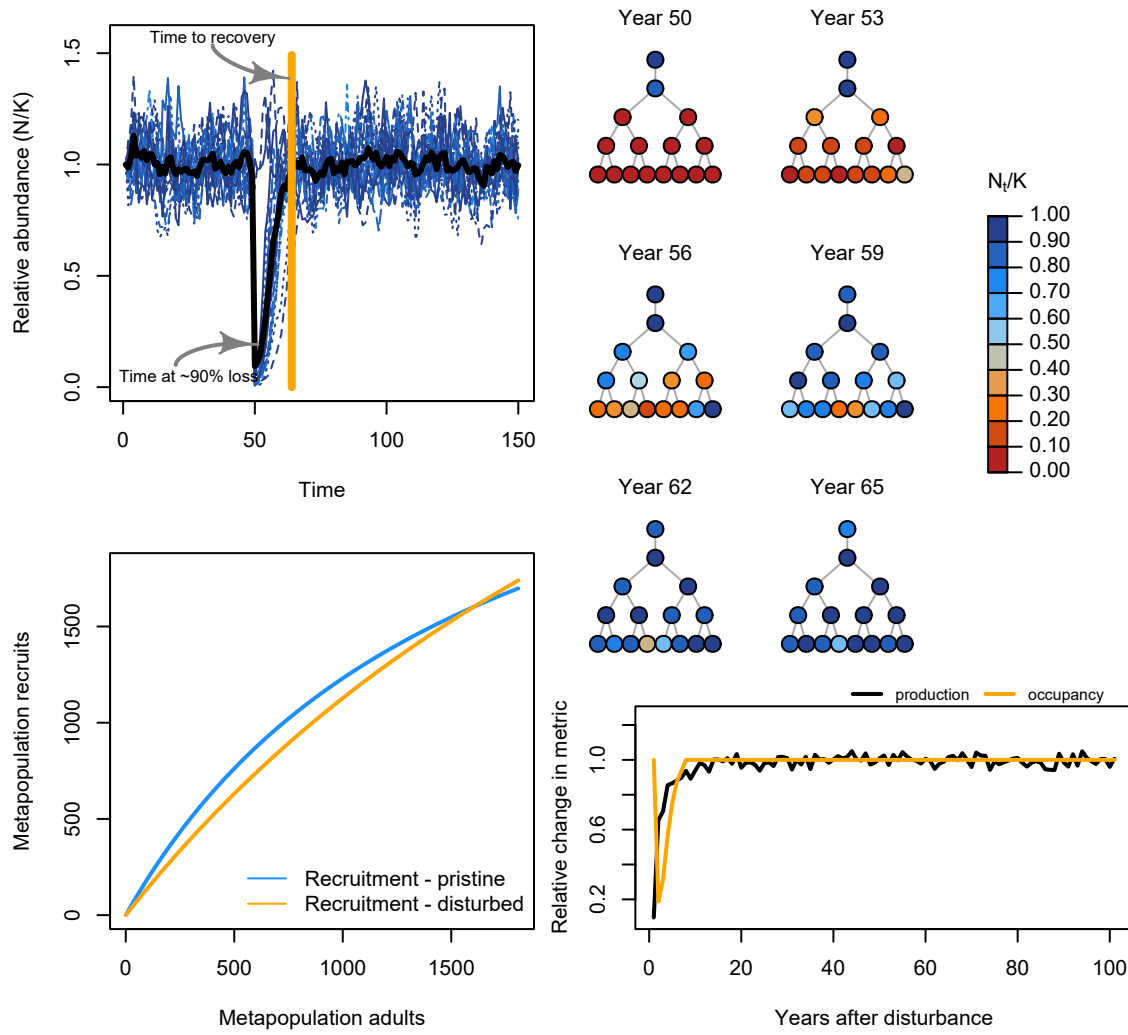


Figure S10: Example iteration of spatial recovery regime of stochastic metapopulation.

188 Next, we can contrast with a disturbance regime where the disturbance is concentrated on local patches that can
 189 be completely extirpated (rather than the disturbance being applied proportionally across all patches e.g., a
 190 mixed-stock fishery).

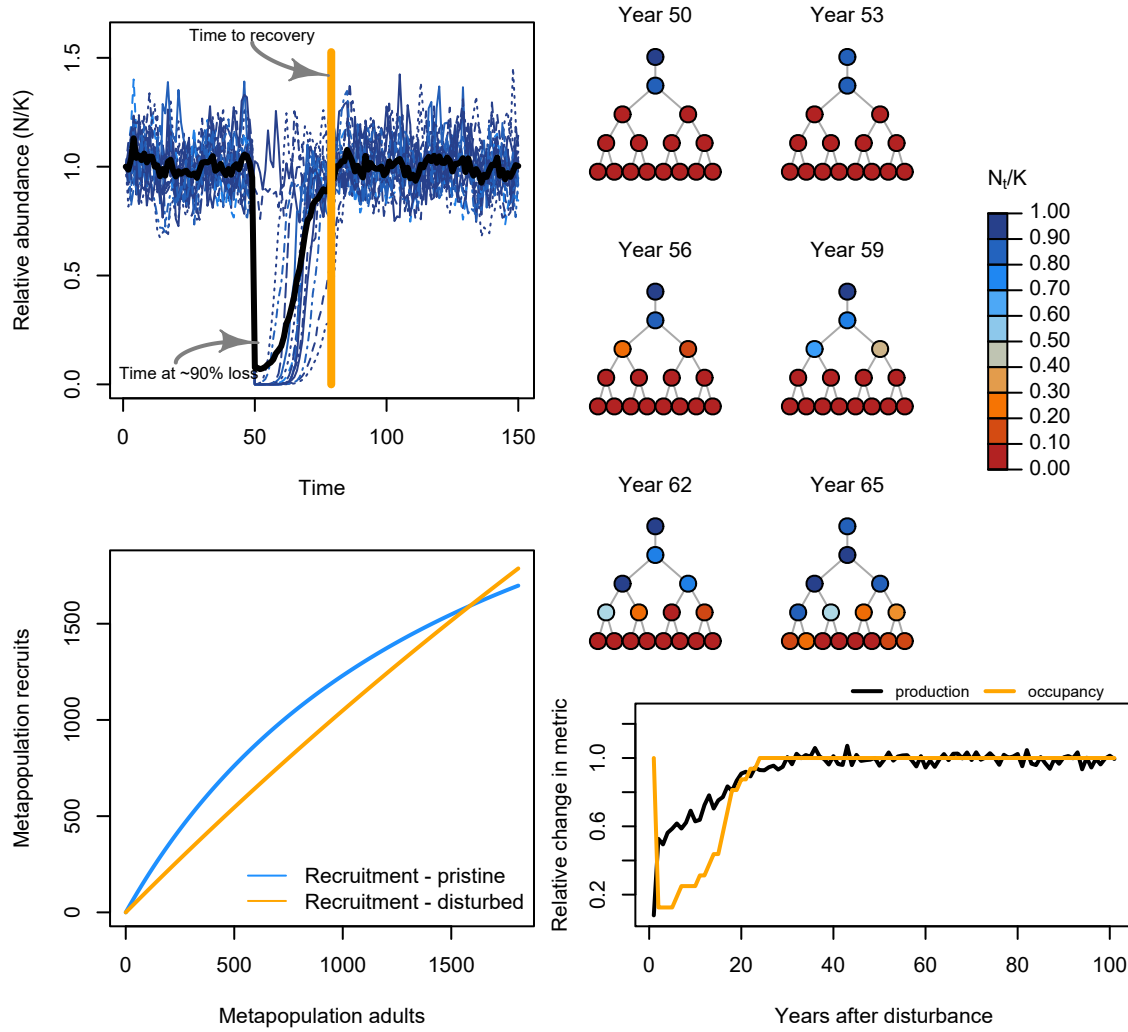


Figure S11: Example iteration of spatial recovery regime of stochastic metapopulation.

191 S1.4 Sensitivity test of mean recovery metrics

192 The total number of scenarios resulted in a long computation time to run all simulations a large number of times
 193 necessary to evaluate how metapopulation responded, on average, to our ecological and disturbance scenarios. To
 194 determine a sufficient number of bootstrap iterations to run, we ran a sensitivity test to explore the relative
 195 sensitivity of the mean for a few recovery metrics of interest (recovery rate) to the number of stochastic simulations
 196 ran per scenario. Below, we repeated the scenario for a metapopulation with a dendritic network, with high
 197 stochasticity, locally uneven disturbances, large spatial-temporal correlations, variable patch productivities, and
 198 variable patch capacities along gradients of 10, 100, 500, and 1,000 stochastic simulations. Based on these
 199 preliminary results, we see that the mean for most metrics was relatively insensitive with at least 100 simulations.

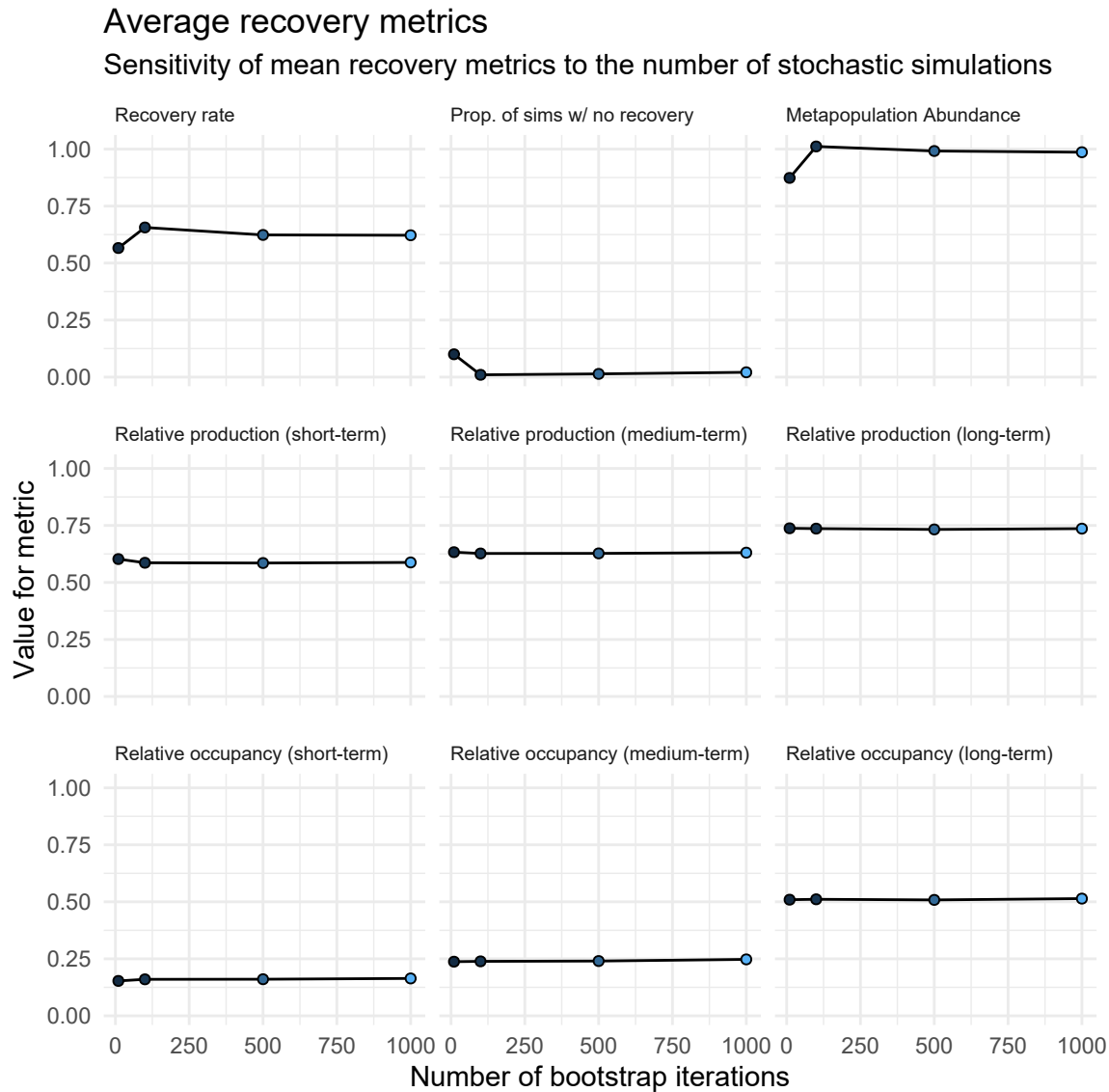


Figure S12: Sensitivity test of mean recovery metrics to number of iterations to bootstrap the stochastic simulations. Example metapopulation consisted of a dendritic network, high recruitment stochasticity, locally uneven disturbance regime, large spatial-temporal correlations, variable patch productivities, and variable patch capacities tested along gradients of 10, 100, 500, and 1,000 bootstrapped iterations.

200 S1.5 General patterns

201 S1.5.1 Effects of disturbance regime

202 The strongest lever influencing recovery in our simulated metapopulations was, by far, the characteristics of the
 203 disturbance regime. Specifically, the degree to how locally concentrated the disturbance was on the set of patches
 204 was more influential than variation in local demographic rates, dispersal rates, or network topology. Localized
 205 disturbances increased the risk of spatial contraction, reduced recovery rates and aggregate compensation, and
 206 increased the risk of non-recoveries. By altering aggregate compensation, localized disturbance reduced the relative
 207 production of the metapopulation. In other words, through changes in source-sink dynamics, metapopulations
 208 under localized disturbance acted less than the sum of their parts – the more localized the impacts, the worse these
 209 effects. Uniform disturbances generally left the metapopulation dynamics unaffected with few changes to recovery
 210 metrics outside of occasionally slower recoveries. These above spatial and temporal recovery processes also
 211 appeared tied to one another such that changes to any of them had feedbacks with other recovery metrics. Perhaps
 212 intuitively, for example, patch occupancy was highly correlated to the relative production of the metapopulation,
 213 such that the more patches occupied, the more that metapopulation dynamics resembled a contiguous population.

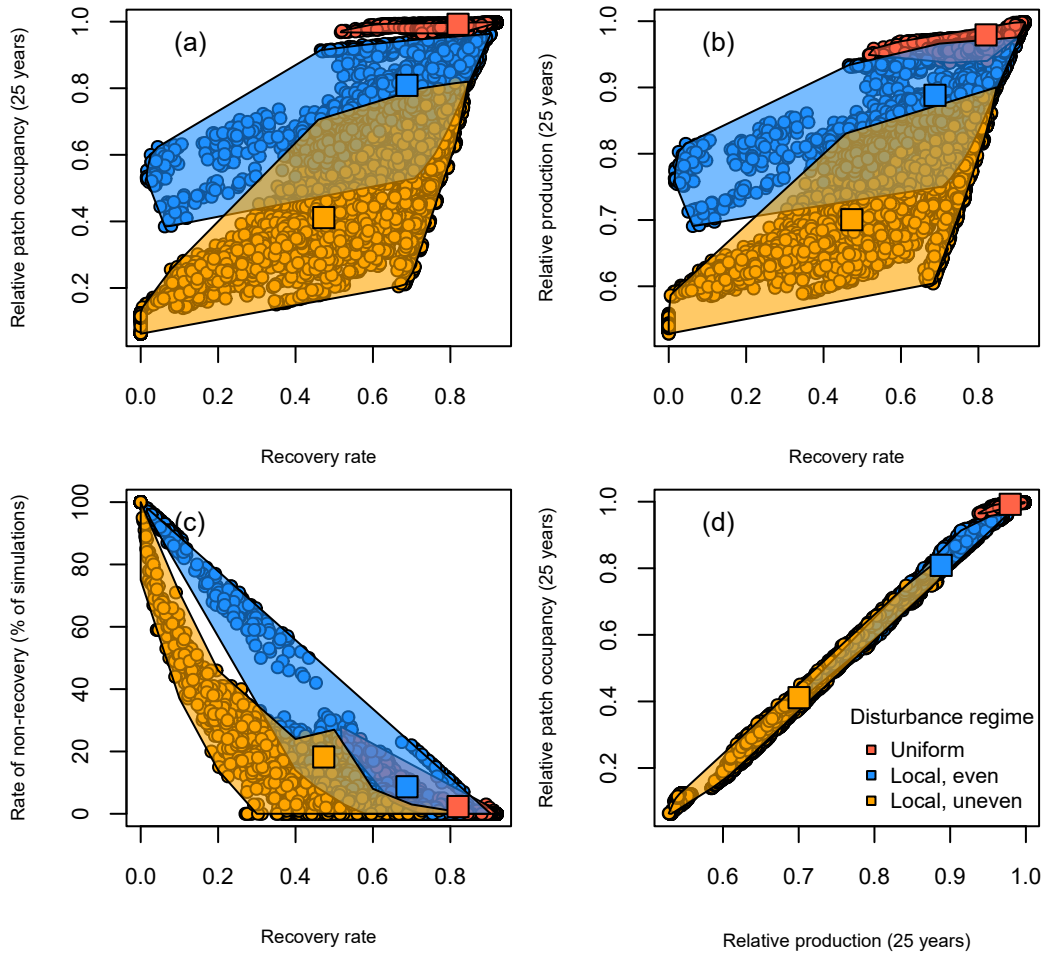


Figure S13: The role of spatial disturbance regimes on metapopulation recoveries and covariation among four recovery metrics: (a,b,c) recovery rate – the annual rate of metapopulation recovery; (a,d) relative patch occupancy – the mean proportion of patches occupied 25 years after disturbance; (b,d), relative production – the ratio between the summed abundances across all patches to the expected production of an equivalent single population 25 years after disturbance; and (c) rate of non-recovery – the percent of 100 stochastic simulations where the metapopulation failed to recover. Each point represents a single simulation for a metapopulation under a unique combination of local productivity, dispersal, spatial network, stochasticity, and disturbance (9,504 total simulations). Shaded regions describe the range in recovery metrics for all simulated metapopulations and are colored by disturbance regime. Square points represent the mean recovery metrics from all simulations within each disturbance regime.

²¹⁴ **S1.5.2 Role of interplay in ecological and disturbance conditions on recovery patterns**

²¹⁵ We now show some general patterns in how variable patch demographic rates, network structure, dispersal,
²¹⁶ disturbance, recruitment stochasticity, and spatio-temporal correlations variation affects metapopulation *recovery*
²¹⁷ rates (shown in Figure 4 of the main text and Figure S13 & S15), *non-recovery rate* (i.e., the number of simulations
²¹⁸ where the metapopulation fails to recover; Figure S16), *patch occupancy* (i.e., number of patches with local
²¹⁹ abundance <10% of pre-disturbance; Figure S17), and *relative production* (Figure S18).

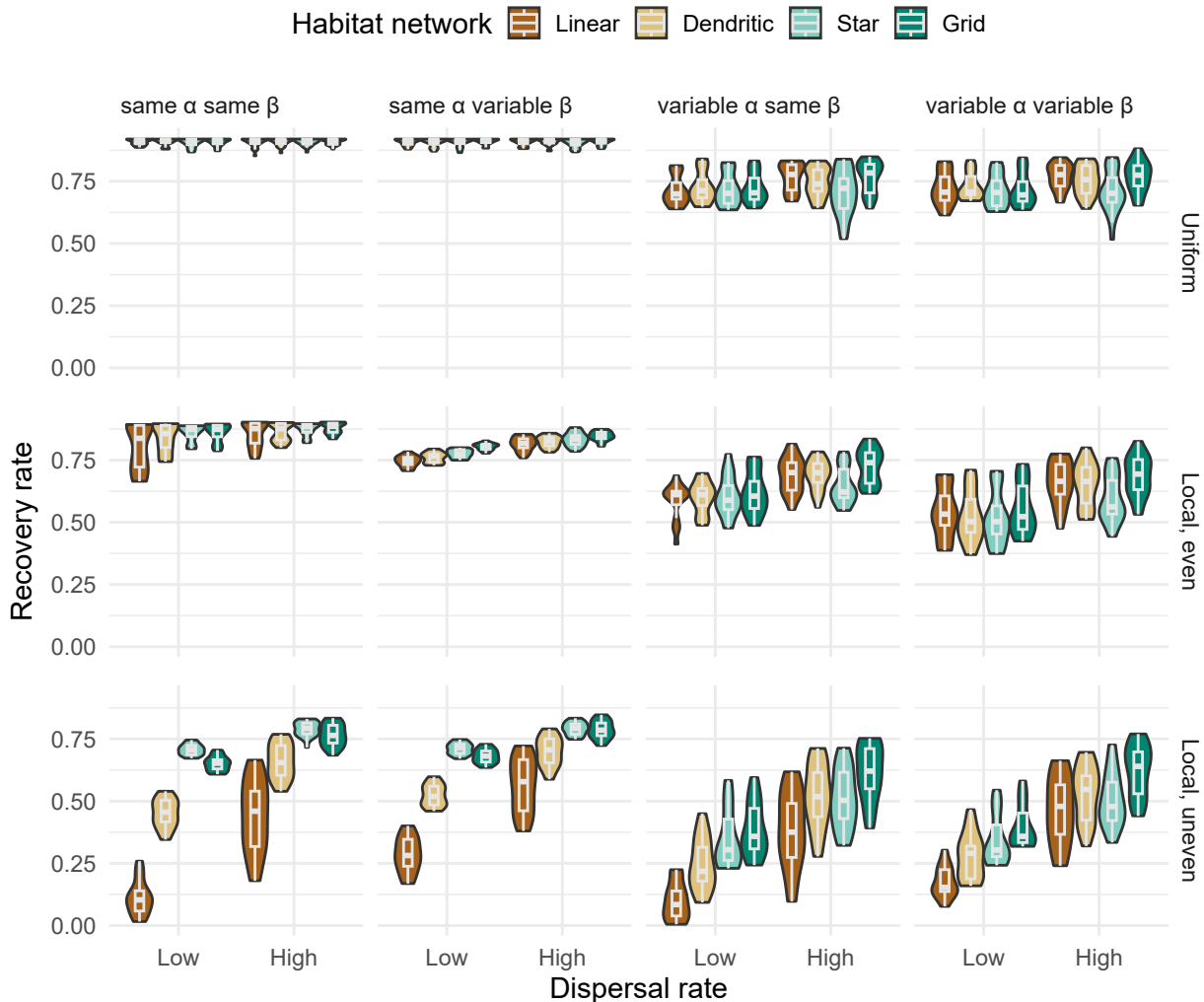


Figure S14: Violin plots showing marginal response of metapopulation recovery rates along gradients of network configuration, dispersal categories (low 0.001; high >0.001), heterogeneity in local demographic rates (α was local patch productivity and β was local patch carrying capacity in the Beverton-Holt model), and spatial distribution of disturbance.

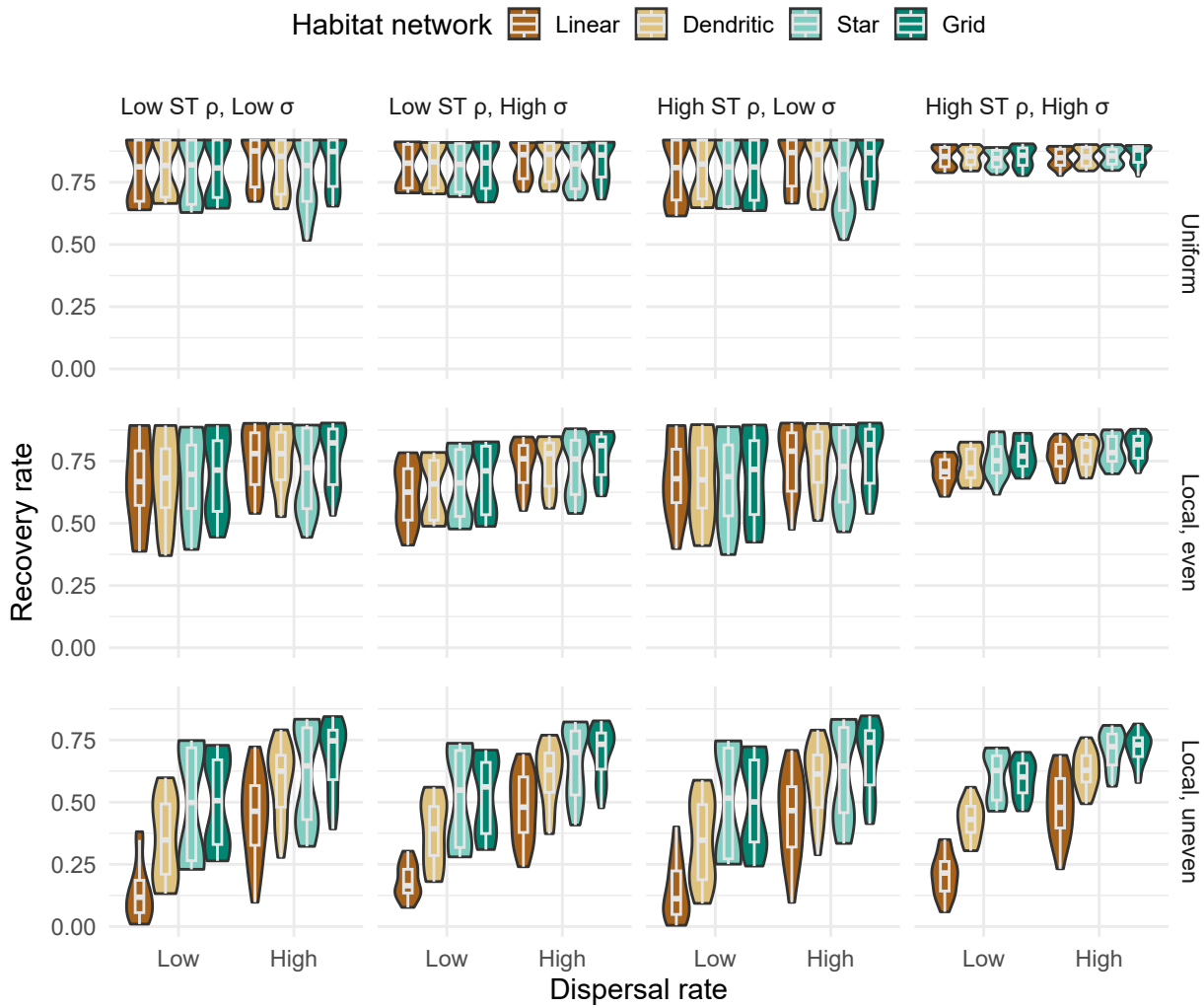


Figure S15: Violin plots showing marginal response of metapopulation recovery rates along gradients of network configuration, dispersal categories (low 0.001; high > 0.001), spatial-temporal (ST) correlations (low $\rho = 0$; high $\rho = 0.6$), scale of lognormal variance in recruitment (low $\sigma = 0.001$; high $\sigma = 0.1$), and spatial distribution of disturbance.

220 Next, we show violin plots demonstrating some of the modulating factors leading to variation in the risk of
 221 non-recovery owing to stochastic recruitment dynamics.

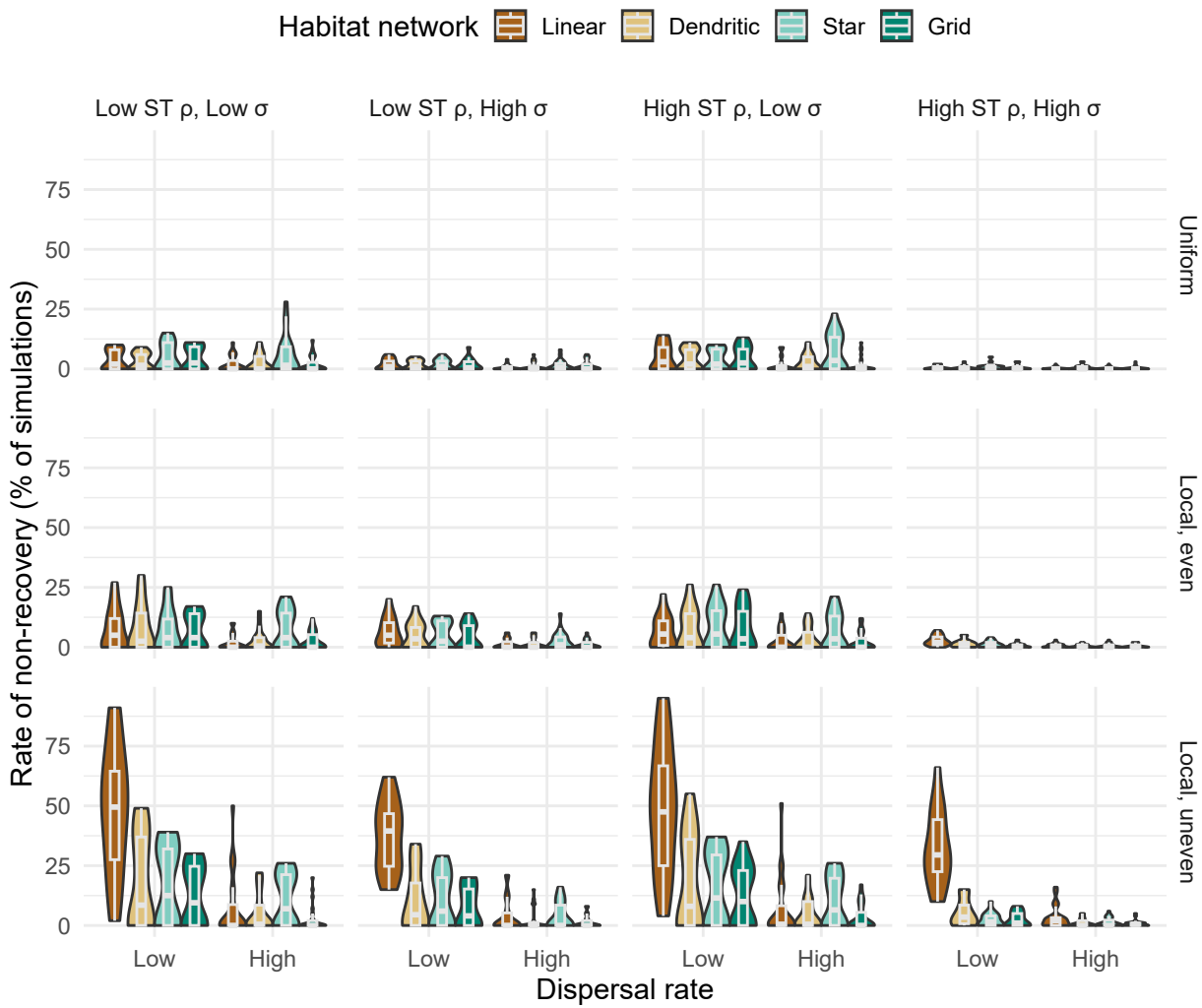


Figure S16: Violin plots showing marginal response of the stochastic risk of non-recovery in metapopulations along gradients of network configuration, dispersal categories (low 0.001; high > 0.001), spatial-temporal (ST) correlations (low $\rho = 0$; high $\rho = 0.6$), scale of lognormal variance in recruitment (low $\sigma = 0.001$; high $\sigma = 0.1$), and spatial distribution of disturbance.

222 Next, we show violin plots demonstrating some of the modulating factors leading to variation in long-term impacts
 223 to patch occupancy.

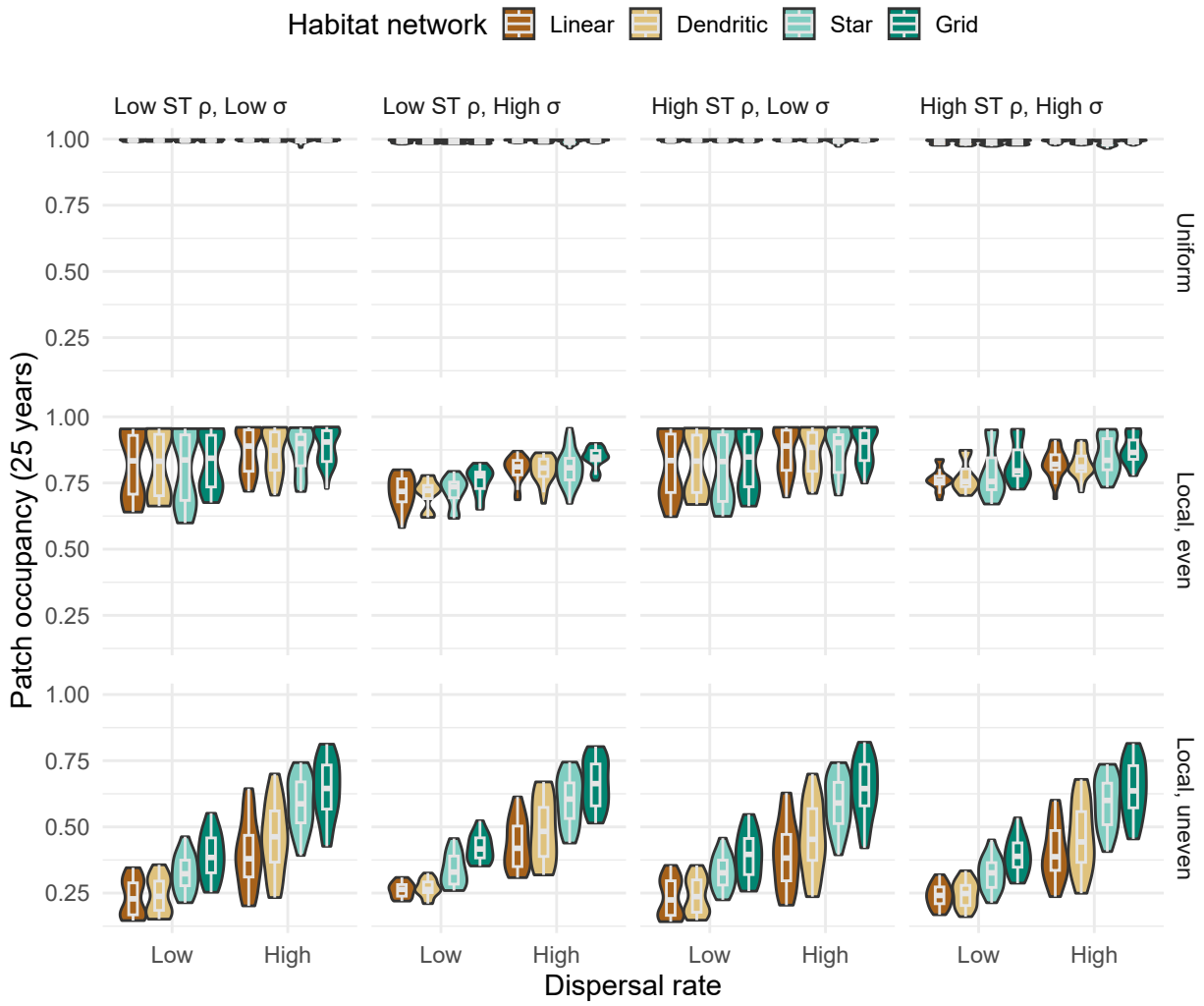


Figure S17: Violin plots showing marginal response of long-term patch occupancy in metapopulations along gradients of network configuration, dispersal categories (low 0.001; high >0.001), spatial-temporal (ST) correlations (low ρ 0; high $\rho=0.6$), scale of lognormal variance in recruitment (low $\sigma= 0.001$; high $\sigma=0.1$), and spatial distribution of disturbance.

²²⁴ Next, we show variation in relative production metrics. Figure S13 shows the tight correlation between patch
²²⁵ occupancy and relative production. Hence, Figure S17 and S18 look quite similar.

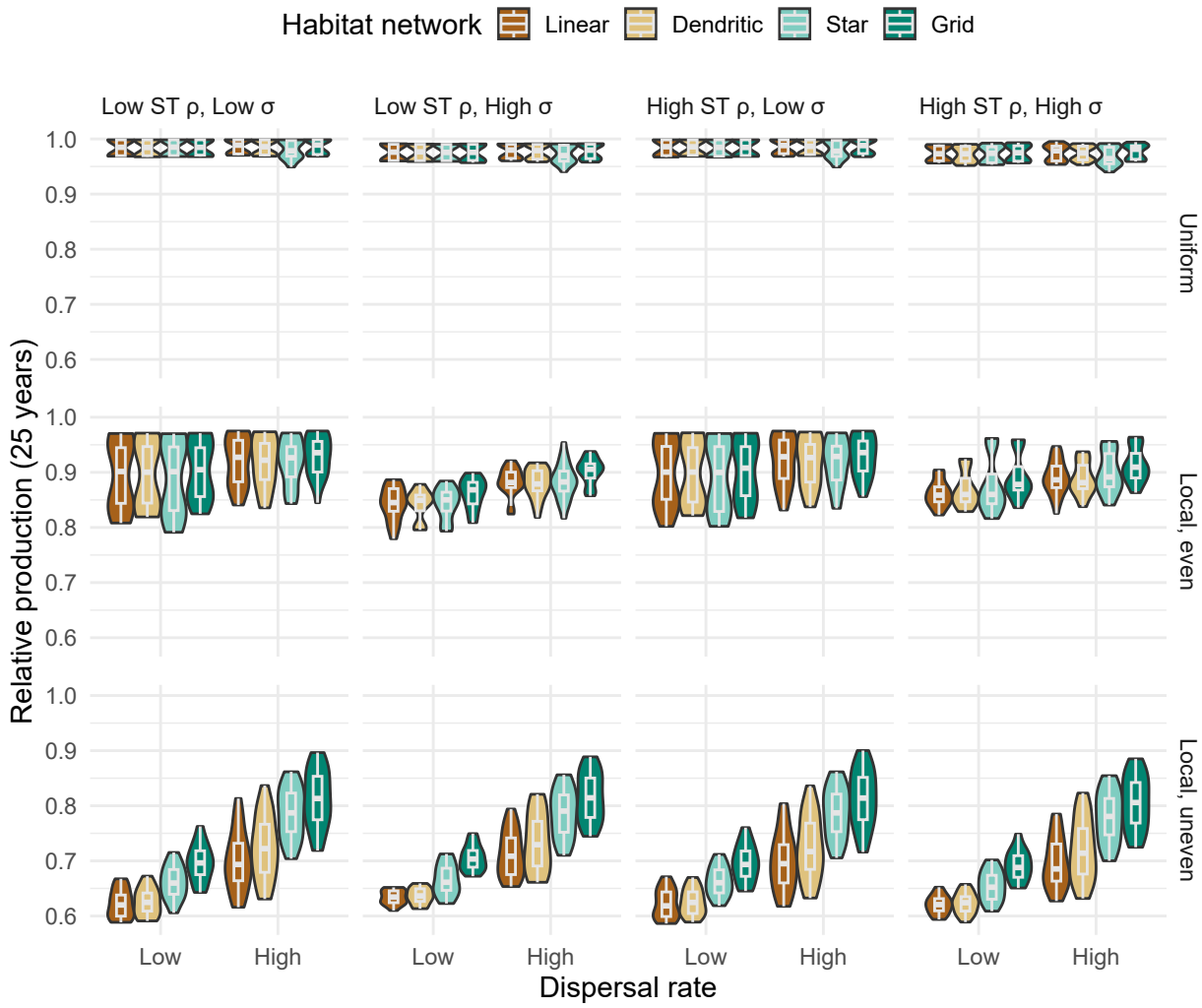


Figure S18: Violin plots showing marginal response of relative production for metapopulations along gradients of network configuration, dispersal categories (low 0.001; high >0.001), spatial-temporal (ST) correlations (low ρ 0; high $\rho=0.6$), scale of lognormal variance in recruitment (low $\sigma= 0.001$; high $\sigma=0.1$), and spatial distribution of disturbance.

226 Dispersal, network topology, variable local demography, spatial-temporal correlations, and recruitment stochasticity
 227 also affected metapopulation recovery patterns in three key ways, though to a lesser extent. First, recovery rates
 228 increased with increased dispersal. However, this effect was nonlinear with diminishing benefits of dispersal
 229 occurring at ~1-3%, depending on spatial structure and disturbance. Second, more linearized networks had slower
 230 recovery times than more connected networks suggesting that rescue effects take some time to cascade through the
 231 entire network of patches; but this interacted with the disturbance regime as only local, extirpation exhibited this
 232 change in any substantial manner. Last, diversity in local patch compensation and carrying capacities tended to
 233 slow metapopulation recoveries - this effect interacted with other factors like stochasticity.

234 S1.6 Clustering analyses

235 We used hierarchical clustering analyses (implementing Ward's criterion) of a dissimilarity matrix from our four
 236 recovery metrics to evaluate whether there was evidence for common recovery regimes among our simulation results
 237 across all ecological and disturbance scenarios (Murtagh & Legendre 2014). Based on advice laid out in Hennig
 238 (2014), we determined that the best number of unique clusters in metapopulation recoveries should satisfy the
 239 following statistical criteria:

- 240 1. recovery outcomes from within a cluster are closer to one another than to other clusters (i.e., the two Dunn
 241 indices are relatively high)
 242 2. the number of clusters explains much of the point variation within the dataset (i.e., diminishing returns in
 243 minimizing the sums-of-squared residuals)
 244 3. the point observations within clusters are relatively tight (i.e., both the average silhouette width and the
 245 widest within-cluster gap are relatively low)
 246 4. clusters are relatively unique and there is good separation between the clusters (i.e., the separation index is
 247 still high, while considering that low numbers of clusters should always have the highest separation)

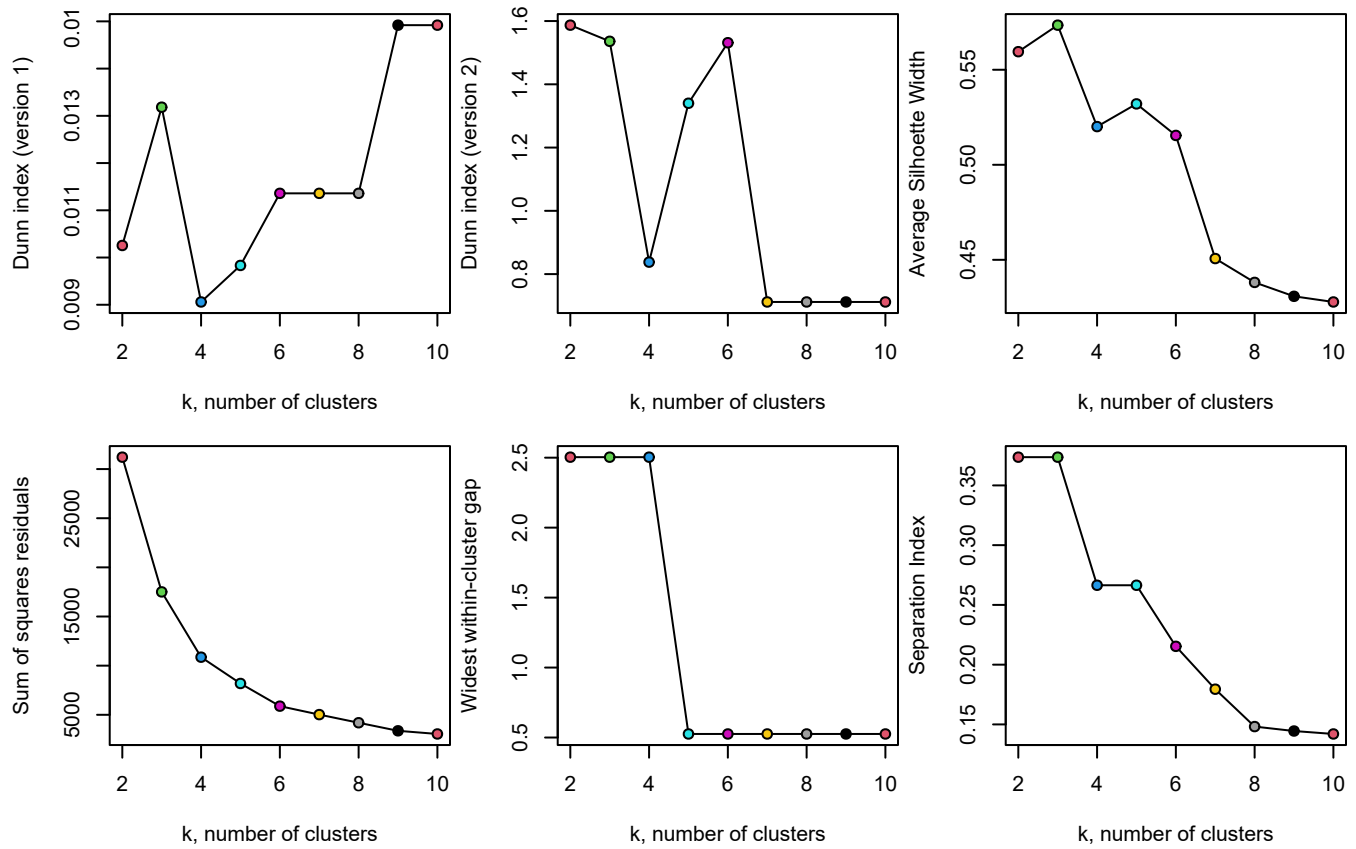


Figure S19: The relationships between number of potential clusters and multiple statistical criteria used to test support for the best number of clusters within the simulated recovery outcomes.

248 Based on the above criteria, we chose 5 unique clusters as satisfying most of the above criteria in the figure above,
 249 although there was good support for between 3 and 6 unique clusters. The principal components analysis indicates
 250 that five clusters has substantial explanatory power of metapopulation recovery metrics (explained ~89% of the
 251 point variation).

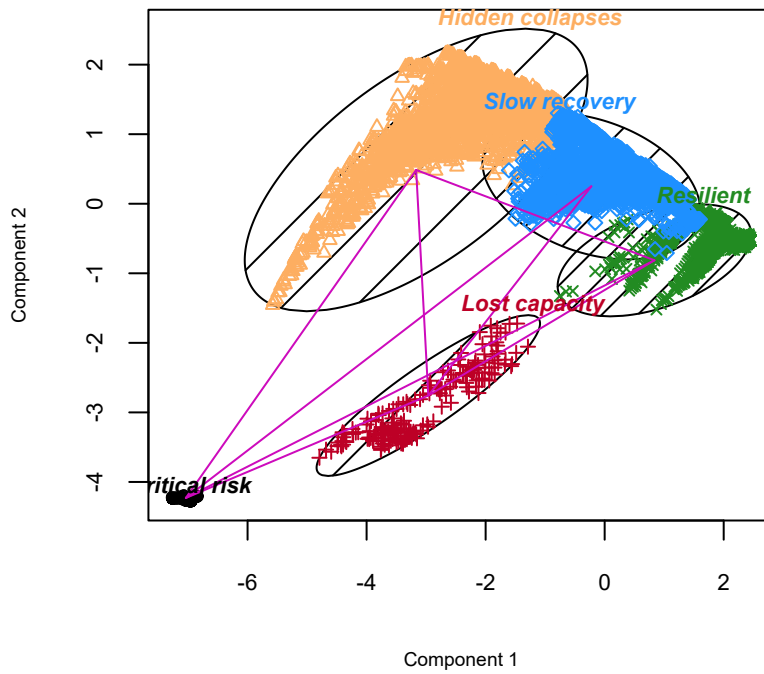


Figure S20: Bivariate cluster plot of the principal components explaining point variation in metapopulation recovery metrics across all simulated scenarios grouped into five distinct clusters.

252 S1.6.1 Emergent recovery outcomes

253 Overall, we used hierarchical clustering analyses to describe five common metapopulation recovery outcomes. These
 254 outcomes were: (1) resilient recovery – metapopulations recovered to pre-disturbance abundances quickly with all
 255 patches occupied, (2) slow recovery – were either slowed (compared to resilient recoveries), had reduced patch
 256 occupancy, or reduced relative production, (3) hidden collapses – metapopulations tended to recover and aggregate
 257 abundances were high, but many local patches remained unoccupied and recovery was slowed, (4) lost capacity –
 258 recovery rates were very slow, the risk of non-recovery was high, long-term production was low, and many local
 259 patches remained unoccupied and (5) critical risk – where metapopulations failed to recover, abundances remained
 260 low, and the risk of non-recovery was high.

Table S2: The mean recovery metrics, total sample size per regime (No.), and metapopulation abundance (N/K) for each of five common metapopulation recovery regimes supported by hierarchical clustering analyses across gradients in disturbance and network structure.

Regime	Network	Disturbance	No.	Recovery rate	% non-recovery	Occupancy	Relative production	Relative abundance
Resilient	Linear	Uniform	792	0.83	2	0.99	0.98	1.00
Resilient	Dendritic	Uniform	792	0.82	2	0.99	0.98	0.99
Resilient	Star	Uniform	792	0.81	3	0.99	0.98	0.99
Resilient	Grid	Uniform	792	0.82	2	0.99	0.98	1.00
Resilient	Linear	Local, even	205	0.78	5	0.94	0.95	0.99
Resilient	Dendritic	Local, even	201	0.78	5	0.94	0.96	0.99
Resilient	Star	Local, even	274	0.75	7	0.93	0.95	0.99
Resilient	Grid	Local, even	215	0.78	5	0.94	0.96	0.99
Slow recovery	Linear	Local, even	528	0.69	3	0.77	0.87	0.99
Slow recovery	Dendritic	Local, even	533	0.70	3	0.77	0.87	0.99
Slow recovery	Star	Local, even	466	0.68	5	0.75	0.86	0.99
Slow recovery	Grid	Local, even	529	0.73	3	0.81	0.89	0.99
Slow recovery	Linear	Local, uneven	11	0.72	0	0.64	0.81	1.00
Slow recovery	Dendritic	Local, uneven	69	0.73	0	0.66	0.81	0.99
Slow recovery	Star	Local, uneven	114	0.74	4	0.71	0.84	0.97
Slow recovery	Grid	Local, uneven	244	0.76	0	0.73	0.85	1.00

Hidden collapses	Linear	Local, even	9	0.61	3	0.59	0.79	0.99
Hidden collapses	Dendritic	Local, even	9	0.65	0	0.59	0.78	0.99
Hidden collapses	Star	Local, even	4	0.72	0	0.55	0.76	1.00
Hidden collapses	Linear	Local, uneven	709	0.34	21	0.34	0.67	0.97
Hidden collapses	Dendritic	Local, uneven	651	0.49	8	0.36	0.68	0.99
Hidden collapses	Star	Local, uneven	606	0.57	9	0.45	0.72	0.99
Hidden collapses	Grid	Local, uneven	476	0.56	7	0.46	0.73	0.99
Lost capacity	Linear	Local, even	50	0.17	77	0.58	0.79	0.66
Lost capacity	Dendritic	Local, even	49	0.16	78	0.58	0.78	0.65
Lost capacity	Star	Local, even	48	0.16	78	0.58	0.78	0.65
Lost capacity	Grid	Local, even	48	0.16	79	0.57	0.78	0.64
Critical risk	Linear	Local, uneven	72	0.00	100	0.10	0.54	0.09
Critical risk	Dendritic	Local, uneven	72	0.00	100	0.10	0.54	0.08
Critical risk	Star	Local, uneven	72	0.00	100	0.10	0.54	0.08
Critical risk	Grid	Local, uneven	72	0.00	100	0.10	0.54	0.08

261 In general, the five recovery regimes spanned a continuum of better (e.g., resilient) to worse recoveries (e.g.,
 262 long-term critical risks). Overall, the interplay between ecological and disturbance conditions appeared to structure
 263 the specific pathway for metapopulation recoveries (Figure S21; Table S2). For example, uniform disturbances
 264 always led to resilient recoveries. However, local, even disturbance regimes tended to lead to, at-best, a resilient
 265 recovery or, at worst, hidden collapses with the probability modulated by other ecological factors. Local, uneven
 266 disturbance regimes led to, at best, a slow recovery or, at worst, a long-term critical risk and non-recovery. The
 267 main text Figure 5 and 6 demonstrates the conditions that led to resilient recoveries compared to critical risks,
 268 while more intermediate outcomes, like slow recovery, hidden collapses, or lost capacity are shown here in Figures
 269 S22-S24.

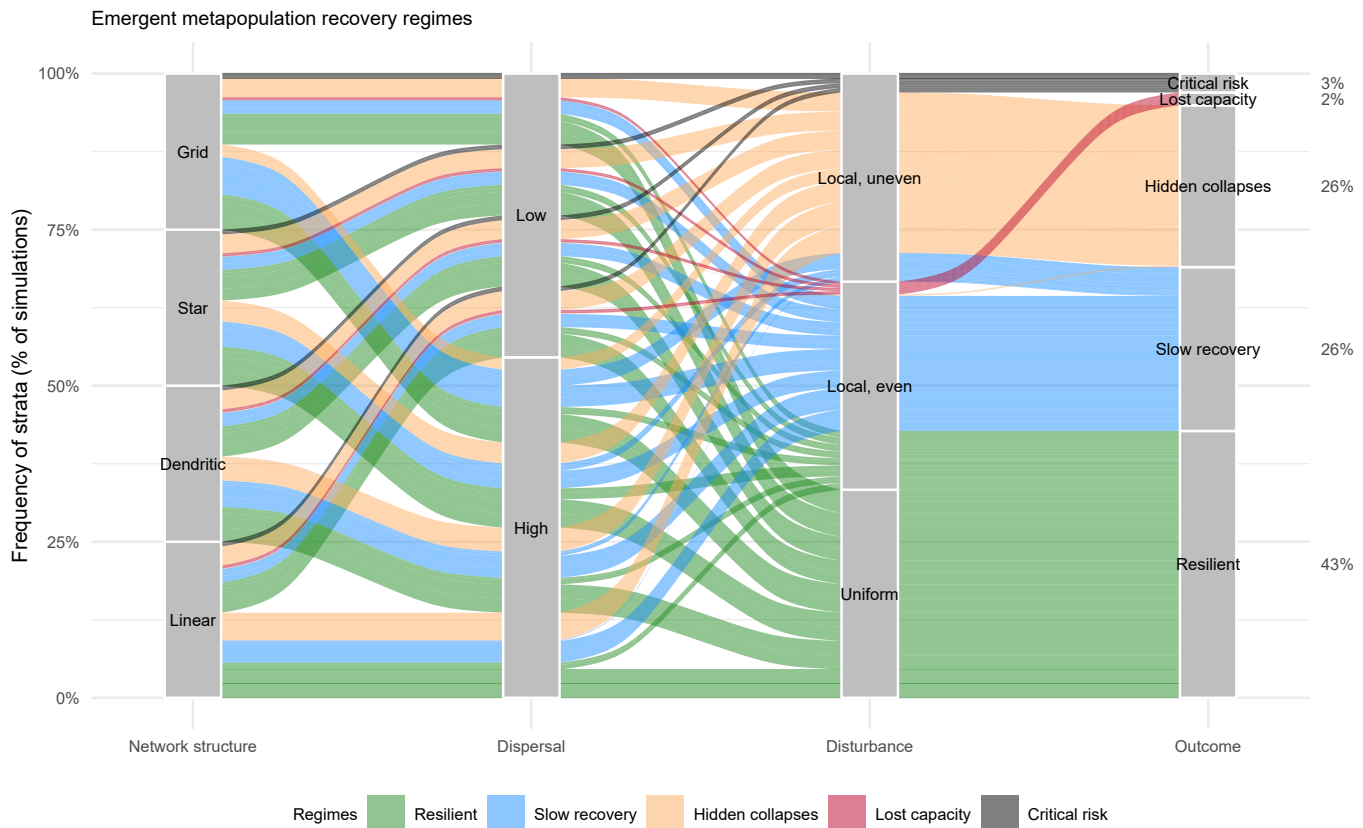


Figure S21: Frequency of emergent metapopulation recovery regimes can depend on a complex interplay between network structure, dispersal, and spatial disturbances. Ribbon colors denote a group of simulations that led to one of five common recovery outcomes. Frequency of regimes denoted by width of ribbons

270 S1.6.2 Role of ecological and disturbance conditions on recovery outcomes

271 Local patch demography, habitat network structure, dispersal, spatially and temporally correlated recruitment
 272 variation, and spatial disturbance regimes each had modulating effects on the probability for any particular
 273 recovery regime (Figures 5 & 6 in the main text; and Figures S22-S24 here). There was a clear signal from any
 274 localized disturbances, which increased the probability for non-resilient recovery regimes. For habitat networks,
 275 metapopulations with linear networks tended to have increased probability for worse recoveries compared to
 276 gridded networks. For dispersal rates, metapopulations with low dispersal had increased probability for poor
 277 recoveries compared to high dispersal. For local demography, metapopulations with variable local patch
 278 demographic rates tended to increased probability for poor recoveries compared to metapopulations composed of
 279 homogeneous local patches. For recruitment stochasticity, metapopulations with both high recruitment variation
 280 and high spatial-temporal correlations led to increased probability for poor recoveries compared to low variation
 281 and low correlations.

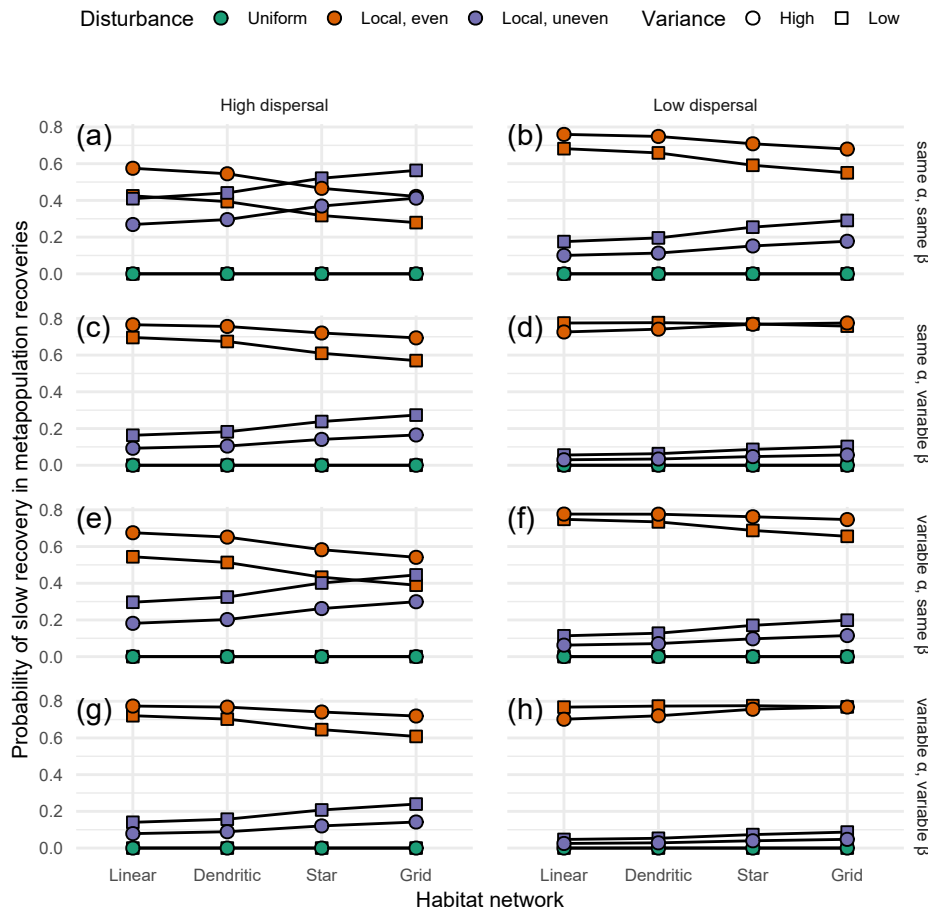


Figure S22: The probability of a slow recovery in metapopulation recoveries depended on the interplay between network structure, dispersal (low 0.001; high > 0.001), spatial disturbances, heterogeneity in local demographic rates (α is local patch productivity and β is local patch carrying capacity), and spatial-temporal recruitment variation (high = $\rho = 0.6$ and $\sigma = 0.1$; low = $\rho = 0$ and $\sigma = 0.001$) based on ordered logistic regression.

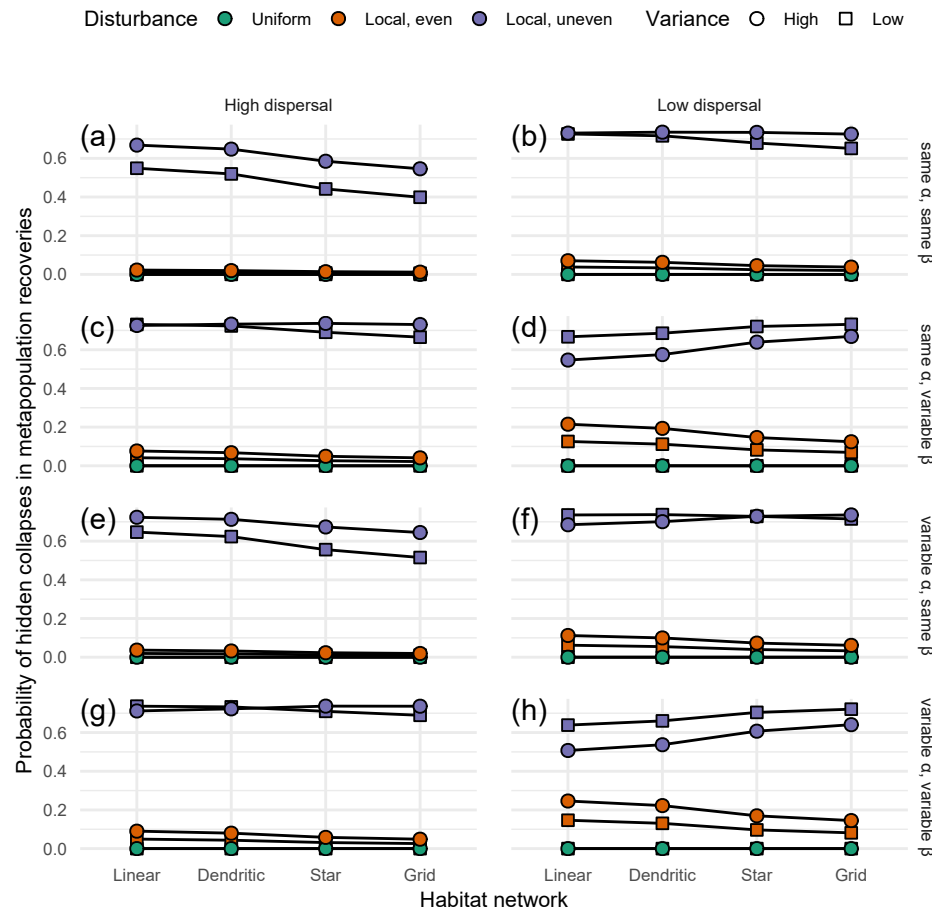


Figure S23: The probability of hidden local collapses in metapopulation recoveries depended on the interplay between network structure, dispersal (low 0.001; high > 0.001), spatial disturbances, heterogeneity in local demographic rates (α is local patch productivity and β is local patch carrying capacity), and spatial-temporal recruitment variation (high = $\rho=0.6$ and $\sigma=0.1$; low = $\rho=0$ and $\sigma=0.001$) based on ordered logistic regression.

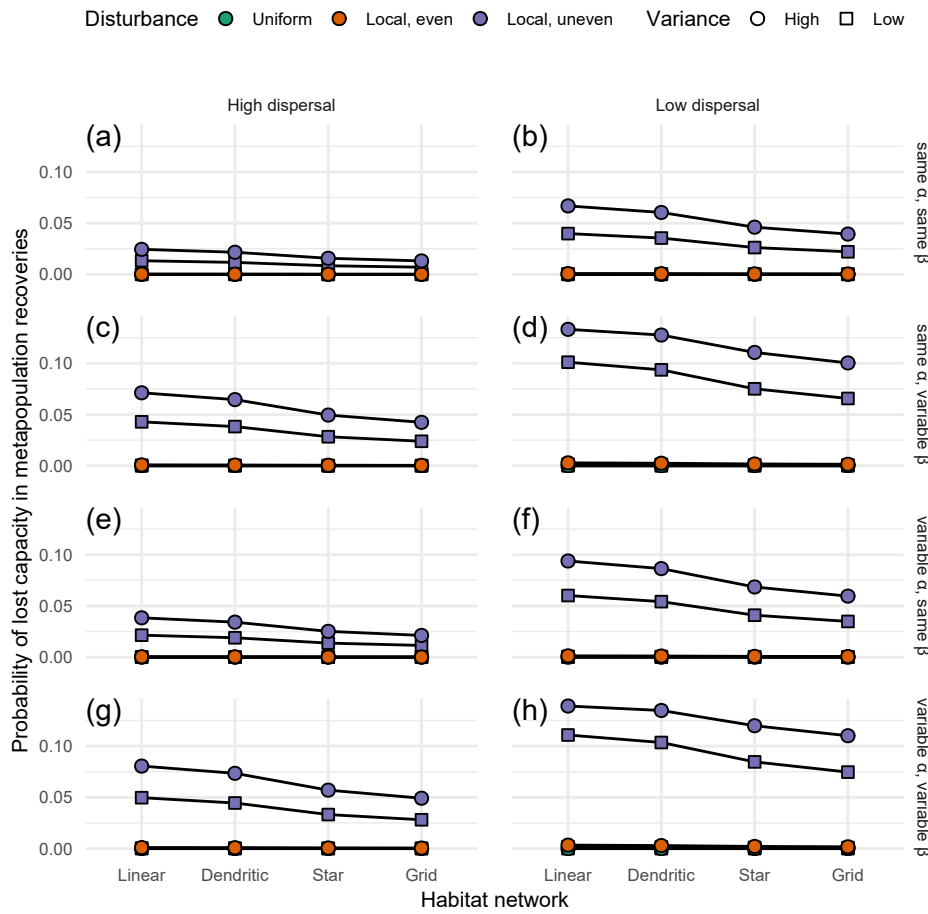


Figure S24: The probability of lost productive capacity in metapopulation recoveries depended on the interplay between network structure, dispersal (low 0.001; high > 0.001), spatial disturbances, heterogeneity in local demographic rates (α is local patch productivity and β is local patch carrying capacity), and spatial-temporal recruitment variation (high = $\rho=0.6$ and $\sigma=0.1$; low = $\rho=0$ and $\sigma=0.001$) based on ordered logistic regression.

282 S1.7 References

- 283 Anderson, S.C., Moore, J.W., McClure, M.M., Dulvy, N.K. & Cooper, A.B. (2015). Portfolio conservation of
284 metapopulations under climate change. *Ecological Applications*, 25, 559–572.
285 Bowlby, H.D. & Gibson, A.J.F. (2020). Evaluating whether metapopulation structure benefits endangered
286 diadromous fishes. *Canadian Journal of Fisheries and Aquatic Sciences*, 77, 388–400.
287 Csardi, G. & Nepusz, T. (2006). The igraph software package for complex network research. *InterJournal*,
288 Complex Sy, 1695.
289 Forrest, R.E., McAllister, M.K., Dorn, M.W., Martell, S.J.D. & Stanley, R.D. (2010). Hierarchical Bayesian
290 estimation of recruitment parameters and reference points for Pacific rockfishes (*Sebastodes* spp.) under
291 alternative assumptions about the stock-recruit function. *Canadian Journal of Fisheries and Aquatic Sciences*,
292 67, 1611–1634.
293 Fullerton, A.H., Anzalone, S., Moran, P., Van Doornik, D.M., Copeland, T. & Zabel, R.W. (2016). Setting spatial
294 conservation priorities despite incomplete data for characterizing metapopulations. *Ecological Applications*, 26,
295 2558–2578.
296 Hennig, C. (2014). How many bee species? A case study in determining the number of clusters. In: *Data analysis,
297 machine learning and knowledge discovery* (eds. Spiliopoulou, M., Schmidt-Thieme, L. & Janning, R.). pp.
298 41–49.
299 Moore, J.W., Connors, B.M. & Hodgson, E.E. (2021). Conservation risks and portfolio effects in mixed-stock
300 fisheries. *Fish and Fisheries*, faf.12567.
301 Murtagh, F. & Legendre, P. (2014). Ward's hierarchical agglomerative clustering method: which algorithms
302 implement Ward's criterion? *Journal of Classification*, 31, 274–295.
303 Myers, R.A., Bowen, K.G. & Barrowman, N.J. (1999). Maximum reproductive rate of fish at low population sizes.
304 *Canadian Journal of Fisheries and Aquatic Sciences*, 56, 2404–2419.
305 Okamoto, D.K., Hessing-Lewis, M., Samhour, J.F., Shelton, A.O., Stier, A.C., Levin, P.S. & Salomon, A.K. (2020).

- 306 Spatial variation in exploited metapopulations obscures risk of collapse. *Ecological Applications*, 30, e02051.
307 Walters, C.J. & Martell, S.J.D. (2004). *Fisheries ecology and management*. Princeton University Press.
308 Yeakel, J.D., Moore, J.W., Guimarães, P.R. & Aguiar, M.A.M. de. (2014). Synchronisation and stability in river
309 metapopulation networks. *Ecology Letters*, 17, 273–283.
310 Zelnik, Y.R., Arnoldi, J. & Loreau, M. (2019). The three regimes of spatial recovery. *Ecology*, 100, e02586.